

Impact of axonal delay on structure development in a Linsker-type network

Catherine E. Davey^a, David B. Grayden^{a,b}, and Anthony N. Burkitt^{a,b}

^a*NeuroEngineering Laboratory, Dept. of Biomedical Engineering, The University of Melbourne, Australia*

^b*Centre for Neural Engineering, The University of Melbourne, Australia*

April 12, 2022

Keywords: neural network, rate-based, plasticity, delay, spatial opponent cells

Abstract

In his seminal, three-paper series, Linsker provided a mechanism for how random activity in the visual pathway could give rise to many of the features observed experimentally in the early stages of visual processing. Owing to the complexity of multi-layer models, an implicit assumption in Linsker's and subsequent papers has been that propagation delay is homogeneous and, consequently, plays little functional role in neural behaviour. In this paper, we relax this assumption to examine the impact of axonal distance-dependent propagation delay on neural learning. We show that propagation delay induces low-pass filtering by dispersing the arrival times of spikes from pre-synaptic neurons, providing a natural correlation cancellation mechanism for distal connections. The cut-off frequency decreases as the radial propagation delay within a layer, relative to propagation delay between the layers, increases, introducing an upper limit on temporal resolution. Given that the post-synaptic potential (PSP) also acts as a low-pass filter, we show that the effective time constant of each should enable the processing of similar scales of temporal information. This result has implications for the visual system, in which receptive field size and, thus, radial propagation delay, increases with eccentricity. Furthermore, the network response is frequency-dependent since higher frequencies require increased input amplitude to compensate for attenuation. This concords with frequency dependent contrast sensitivity in the visual system, which changes with eccentricity and receptive field size. We further show that the proportion of inhibition relative to excitation is larger where radial propagation delay is long relative to inter-laminar propagation delay. Finally, we determine the eigenfunctions of both Linsker's network, and the network with propagation delay. We show that the addition of propagation delay stabilizes the leading eigenfunction to changes in homeostatic parameters, and hence stabilizes the resulting receptive field structure. It also reduces the range in the size of the spatial opponent cell's on-center size, providing stability to variations in homeostatic parameters.

1 Introduction

Synaptic plasticity describes the process by which changes to synaptic weights between neurons occur in response to their activity. The development of mathematical models of plasticity has been instrumental in furthering our understanding of the formation of receptive fields of simple cells in the primary visual cortex (V1). Linsker (1986c,b,a) showed how cells sensitive to simple features, such as orientation, can develop across several neural layers in the absence of structured input, demonstrating how spatial structure in cortical connections is sufficient to drive a self-organization learning process. There has subsequently been much progress in our understanding of the plasticity mechanisms that drive the learning of simple features. An important component of this work has been the development of a rigorous mathematical framework from which to interrogate properties of plasticity and neural network development (MacKay and Miller, 1990; Wimbauer et al., 1998).

In establishing this framework, Hebbian learning has been expressed using rate-based or spike-based models of neural activity. Rate-based models have long been a significant focus of research into Hebbian learning; these models determine synaptic weight changes in proportion to correlation between short time averaged pre- and post-synaptic firing rates (Burkitt et al., 2007). In spike-timing-dependent plasticity (STDP) models, weight changes depend on the relative timing between individual spikes from pre- and post-synaptic neurons, differentiating between a presynaptic neuron contributing to a postsynaptic spike and a postsynaptic neuron spiking just prior to a presynaptic neuron. While STDP can capture temporal dynamics on a microsecond timescale (van Hemmen, 2009; Gerstner et al., 1996), rate-based models average out high precision temporal information (Kempster et al., 1999b). However, for input that does not contain high frequency temporal information, correlations between input and output spikes are captured in correlations between rates and, consequently, rate-based and spike-based models are approximately equal. In this case, the primary difference between the models is the spike triggering effect (van Hemmen, 2009), in which a presynaptic neuron's spike is the cause of a postsynaptic neuron's firing. This effect is small for large numbers of weakly correlated inputs (Burkitt et al., 2004, 2007). The use of spike-based models to mathematically capture the mechanisms of Hebbian learning in a network that incorporates both spatial and temporal information would be extremely complex. Therefore, in this work, we use rate-based models of Hebbian learning.

Development of a rigorous mathematical framework to express Hebbian learning on a network scale has been crucial in advancing our understanding of the formation of simple cells and feature maps in the early stages of learning (Miller, 1990). MacKay and Miller (1990) analyzed the stability properties of Linsker's three layer, rate-based network, providing expressions for the first three radial eigenfunctions of synaptic learning. Identifying eigenfunctions is beneficial because each describes an independent synaptic weight structure that contributes to the learning dynamics in proportion with its corresponding eigenvalue. Consequently, the leading eigenfunction with the largest eigenvalue will typically dominate the learned weight structure and thus determines the receptive field learned by the postsynaptic neuron. Receptive field defines both the region in sensory space and the sensory input pattern required to evoke a strong response in a cell. For a cortical neuron, the receptive field is dictated by its presynaptic cells and the strengths of their synaptic connections. MacKay and Miller (1990) demonstrated that a spatial opponent cell has the leading eigenvalue in Linsker's network and so dominates the structure of the resulting receptive field in early layers of learning. Wimbauer et al. (1998) extended Linsker's model to allow for recurrent cortical connections and showed in their derivation of the Cartesian eigenfunctions of neural learning the conditions under which orientation selective cells emerge. Miller (1990) discussed the conditions required for development of ocular dominance in the visual cortex, resulting from correlated lateral geniculate nucleus (LGN) input with structured synaptic connections in a rate-based, three layer network, similar to Linsker's (1986a).

Owing to the complexity of models resulting from multiple layers of structured input, there has been limited work addressing the impact of axonal delay on the development of simple features, with none yet incorporating the impact of delay both within and between layers. Wimbauer et al. (1997) showed the development of direction selective cells in response to a combination of lagged and non-lagged input via empirical simulation, although the impact of propagation delay was assumed to be negligible. Leibold et al. (2001) provided a mathematical description of the evolution of a temporal feature map, highlighting the importance of temporal parameters in the neuron model and learning function but not incorporating spatially dependent delay. Leibold and van Hemmen (2001) showed the evolution of temporal feature maps for sound localization, employing a one-dimensional spatial structure.

An implicit assumption of most of these papers has been that spike propagation is instantaneous or, equivalently, that the inter-laminar distance is sufficiently greater than radial distances between neurons to permit the assumption that propagation time is approximately equal for all spikes received by a neuron, enabling correlation between neural outputs to be evaluated without spatially induced delay. However, experimental work demonstrates that propagation delay is important. For example, Saam and Eckhorn (2000) showed that spike conduction velocity impacts the spatial range of synchronization and the subsequent receptive field sizes of cells. Kremkow et al. (2016) noted the importance of controlling the delay of excitation and inhibition in broadening the range of statistics that sensory cortical neurons can process. The importance of propagation delay has also been highlighted in the context of synaptic plasticity. Eguchi et al. (2014) discuss the role of propagation delay in developing clusters of cells via STDP, while Asl et al. (2017) explore the impact of propagation delay on emerging network structure with STDP as a result of spike arrival order being disrupted. Furthermore, the advantageous arrangement of conduction delay via propagation length or axon diameter to cause coincident spike arrival at postsynaptic neurons has been long noted, such as in the giant squid axons (Pumphrey and Young, 1938) and the barn owl (Carr and Konishi, 1988).

While the importance of spike timing for synaptic plasticity has been well motivated, the modelling of propagation delay to understand its impact on the evolution of receptive field structure is still in its infancy. In this paper, we examine the impact of three-dimensional propagation delay on the emergence of V1 simple cells using Linsker's three-layered network model. We analytically derive an expression for covariance between neurons that incorporates radial propagation delay determined from connectivity radius, spike propagation velocity, and cell density, inter-laminar propagation delay, and an arbitrary post-

synaptic potential (PSP). We show that, where inter-laminar propagation delay is longer than radial propagation delay, the impact of delay on learning is negligible. As radial propagation delay increases, it effectively acts as a low-pass filter, filtering out high frequencies of the covaried inputs by spreading out the arrival time of pre-synaptic signals to the cell, thereby reducing covariance. Given that a PSP also acts as a low-pass filter, we propose that the cut-off frequencies for each will be compatible. This may partly explain the different synaptic time constants found in peripheral and foveal ganglion cells, which can differ by up to a factor of 2 (Zhao et al., 2016). It may also explain why contrast sensitivity is frequency dependent in the periphery, and why the cut-off frequency increases with eccentricity (Virsu et al., 1982). It also provides an insight in to why spatial and temporal frequency processing in the visual cortex are not independent (Zhao et al., 2016; Venkataraman et al., 2017).

We derive a general expression for the eigenfunctions of Linsker’s (1986a) network, and empirically derive an expression for the eigenfunctions of the network with propagation delay. We show that the presence of propagation delay is important to have a stable leading eigenfunction for all homeostatic constants, as well as a sharp boundary between the ON and OFF regions of the spatial opponent cell. Finally, we show that the size of the on-centre compared to the off-surround of the cell is a function of the fixed point mean synaptic weight, which can be determined from the homeostatic constants and covariance between pre-synaptic inputs. For smaller fixed point mean weights there will be relatively fewer excitatory inputs and more inhibitory inputs. This is in agreement with the synaptic arrangement of ganglion cells, which have significantly more inhibitory inputs in the periphery, where the cells are more spread across the lamina and the impact of radial propagation delay will be greatest (Sinha et al., 2017).

This paper is organized as follows. In Section 2.1 we present Linsker’s (1986a) network and the network with propagation delay, neural models, and learning equations. We detail the full set of eigenfunctions for Linsker’s (1986a) network. We then derive an expression for covariance between neurons in the presence of propagation delay and incorporate this result in to the learning equation in Section 3.3. We subsequently determine the fixed point mean weight and exactly specify the on-center of the resulting spatial opponent cells in Section 3.4. Finally, we determine the full set of eigenfunctions for the network with propagation delay in Section 3.6.

2 Methods

2.1 Specification of the network

We employ the topographic network proposed by Linsker (1986a) comprised of three layers, A , B , and C , with feedforward connections from layer A to B and from layer B to C , as illustrated in Fig. 1. We remain faithful to Linsker’s notion of a simple network with a minimal set of assumptions to identify the fundamental principles driving the emergence of cortical structure (Linsker, 1986a). The layers are positioned as planes parallel to one another with neurons equispaced in a square grid within each lamina. Connections between layers are learned sequentially, such that synapses from A to B are learned to maturity before connections from B to C are learned. To aid interpretation of distance metrics, we measure distances across a lamina in terms of number of grid spaces. Connections between layers have a spatial distribution such that nearby neurons in the presynaptic layer are more densely connected to a postsynaptic neuron in the overlying layer.

As the radial distance from the postsynaptic neuron increases, connection density decreases as a Gaussian function of the distance. Define the two-dimensional radial distance of presynaptic neuron, m , from postsynaptic neuron, i , by a vector, (x_{mi}, y_{mi}) . The density of connections from layer A to the subsequent layer B is parameterized by the radius, $(\sigma^{AB})^2$, which is the distance-dependent variance of the Gaussian distributed connection probability, measured in grid spaces, μ^A , to ensure scaling with cell density in the lamina. Consequently, the probability of presynaptic neuron, m , in layer A generating a synaptic connection to postsynaptic neuron, i , in layer B is given by

$$P_N \left((x_{mi}, y_{mi}) ; \frac{1}{2}(\sigma^{AB})^2 \right) = \frac{1}{\pi(\sigma^{AB})^2} \exp \left(-\frac{x_{mi}^2 + y_{mi}^2}{(\sigma^{AB})^2} \right). \quad (1)$$

Note that this definition differs from the standard definition by a factor of $\sqrt{2}$; it has been specifically chosen for later convenience.

Similarly, the distribution of presynaptic connections from layer B to layer C is Gaussian, parameterized by $(\sigma^{BC})^2$. Without loss of generality, we can assume that a layer C cell is in the center of the lamina, and write the probability of a B cell making

a connection to the layer C cell using polar coordinates,

$$p_N((r_{ip}, \theta_{ip}); (\sigma^{BC})^2) = \frac{1}{\pi(\sigma^{BC})^2} \exp\left(-\frac{r_{ip}^2}{(\sigma^{BC})^2}\right), \quad (2)$$

where r_{ip} is the radial distance from the center of the lamina to i and θ_{ip} is the angle to i within the two-dimensional lamina.

The expected number of shared presynaptic inputs between two postsynaptic neurons in layer B can easily be shown to be (see Appendix A for full derivation)

$$\mathbb{E}[N^{BB}(d)] = \frac{(N^{AB})^2}{2\pi(\sigma^{AB})^2} \exp\left(-\frac{(d_{ij}^B)^2}{2(\sigma^{AB})^2}\right), \quad (3)$$

where d_{ij}^B depicts the distance between neurons i and j such that $d_{ij}^B = \sqrt{x_{mi}^2 + y_{mi}^2}$, measured in grid spaces, μ^A .

An action potential takes time to propagate along an axon. It is generally accepted that, for myelinated axons, transmission time is linearly proportional to the distance propagated (Asl et al., 2017). We introduce a model of transmission delay in which delay is a deterministic and linear function of the three-dimensional distance between the presynaptic and postsynaptic neurons, including both inter- and intra-lamina distances, and is inversely proportional to the speed of propagation.

Let the radial distance of a presynaptic neuron, m , in layer A to a postsynaptic neuron, i , in layer B be given by the magnitude of the (x_{mi}, y_{mi}) vector and designated d_{mi}^B . For Gaussian x_{mi} and y_{mi} , this distance is characterized by a Rayleigh distribution, so that if $(\sigma^{AB})^2$ denotes the connection radius of the Gaussian connections, then the radial distance between neurons in the presynaptic layer A connecting to postsynaptic neuron i has distribution $d_{mi}^B \sim \mathcal{Rayl}\left(0, \frac{(\sigma^{AB})^2}{2}\right)$. Furthermore, the probability of neuron m making a synaptic connection to neuron i from a radial distance d_{mi}^B is

$$p_{Rayl}\left(d_{mi}^B; \frac{(\sigma^{AB})^2}{2}\right) \sim \frac{2d_{mi}^B}{(\sigma^{AB})^2} \exp\left(-\frac{(d_{mi}^B)^2}{(\sigma^{AB})^2}\right). \quad (4)$$

Denoting transmission delay between neuron m in layer A and neuron i in layer C by Δ_{mi}^{AB} and assuming an interlaminar distance of d^{AB} , propagation delay from m to i can be expressed as

$$\Delta_{mi}^{AB} = \frac{((d^{AB})^2 + (d_{mi}^B)^2)^{1/2} \mu^A}{v}, \quad (5)$$

where v is the spike propagation velocity and μ^A is the distance between neurons in the lamina in μm . The distance metrics, including d^{AB} and d_{mi}^B , are measured in grid spaces, μ^A , to separate out the effect of cell density from other distance measures such as connectivity radii and inter-lamina distance.

2.2 Neuron model

Analyzing the weight dynamics using an eigenfunction approach requires a linear system; therefore, we employ a Poisson neuron model. Poisson models are simple in that activity is a linear sum of input weighted by synapse strength, and that spike thresholds and reset are not modelled. Although it is a simple model, Kempter et al. (1999a) noted that large networks of integrate-and-fire neurons exhibit Poisson firing characteristics.

The network is driven by spontaneous activity from layer A , modelled as a homogeneous Poisson process with rate, λ^A .

2.2.1 Linsker's neuron model

Using a Poisson model, a neuron, m , in layer A providing feed-forward input to a neuron, i , in layer B , and a neuron, j , in layer B providing feed-forward input to a neuron, p , in layer C , under an assumption of instantaneous propagation, the firing

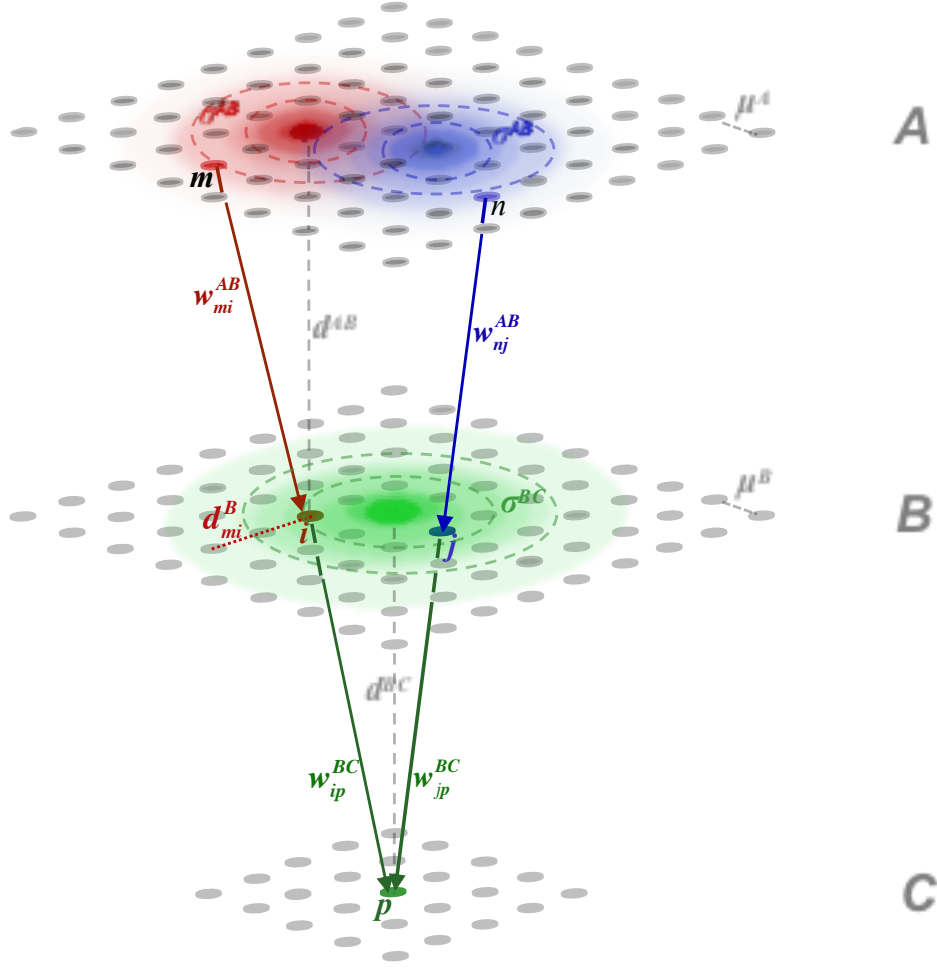


Figure 1: Diagram of a three layer feed-forward network, with neurons m and n in layer A connecting to neurons i and j , respectively, in layer B ; both neurons i and j in layer B connect to neuron p in layer C . Each postsynaptic neuron has been color coded to aid interpretation, such that neuron i has been colored red, neuron j is blue, and neuron p is green. The synaptic connection density of a postsynaptic neuron determines the probability of a neuron in the presynaptic layer connecting to it, and is depicted by the density of that neuron's color in the presynaptic layer. Connection density is modelled as Gaussian, with parameters constant across a layer, so that σ^{AB} denotes the radius, or standard deviation, of connections between layers A and B , while σ^{BC} denotes the radius of connections between layers B and C . The first and second standard deviations of the Gaussian connection probability for a postsynaptic neuron are represented by colored, dashed concentric circles in the presynaptic layer of the neuron. Interlaminar distance between layers A and B is denoted d^{AB} , while distance between layers B and C is denoted by d^{BC} . The radial distance between two neurons within a lamina, for example between neuron m from layer A and i from layer B , is denoted d_{mi}^B . Distance metrics are given in grid spaces, μ^A and μ^B , respectively, which are in themselves measured in μm , to separate out the effect of cell density. The strength of a synaptic connection between two neurons, for example between neurons j and i , is given by w_{ji}^{BC} . Not shown in the diagram are N^{AB} and N^{BC} which represent the expected number of synaptic connections to each postsynaptic neuron in layers B and C , respectively.

rate of the postsynaptic neurons can be described by

$$f_i^B(t) = R_a^B + \sum_m w_{mi}^{AB}(t) f_m^A(t), \quad (6a)$$

$$f_p^C(t) = R_a^C + \sum_j w_{jp}^{BC}(t) f_j^B(t), \quad (6b)$$

where R_a^B denotes background activity and w_{mi}^{AB} depicts synaptic strength between neurons m and i . Note that this differs to Linsker (1986a) by a dimensionless scale factor of R_b^{AB} applied to the sum and which we have absorbed into the weights.

It is useful to introduce frequency domain definitions of the temporal signals. Spectral signals will, in general, be denoted by the upper-case counterpart to the lower-case symbol designating the temporal variable. For example, F_m will denote the frequency domain variable of neuronal rate, f_m . From the definition of the Fourier transform and under the assumption of stationarity (i.e. slow weight evolution), the unfiltered rate can be expressed as a function of spectral variates using the inverse Fourier transform,

$$f_m^B(t) = \frac{1}{T} \sum_k F_m^B(k) \exp\left(2\pi i t \frac{k}{T}\right), \quad F_m^B(k) = \sum_t f_m^B(t) \exp\left(-2\pi i t \frac{k}{T}\right), \quad (7)$$

where \sum_k and \sum_t are shorthand notations for $\sum_{k=0}^{T-1}$ and $\sum_{t=0}^{T-1}$, respectively, to aid readability.

2.2.2 Network incorporating propagation delay and a general postsynaptic response

To model the temporal dynamics of a synapse's membrane potential, we introduce the post-synaptic potential (PSP), ε . For rate-based neuronal activity, this can be interpreted as spikes having a probability distribution over time rather than being modelled by a delta function. For example, the spiking rates from Eq. (6) are generalized to incorporate an arbitrary PSP by

$$(f_i^B \star \varepsilon)(t) = R_a^B + \sum_m w_{mi}^{AB} (f_m^A \star \varepsilon)(t), \quad (8a)$$

$$(f_p^C \star \varepsilon)(t) = R_a^C + \sum_i w_{ip}^{AC} (f_i^B \star \varepsilon)(t), \quad (8b)$$

where \star is the convolution operator and $(f_i^B \star \varepsilon)$ denotes neuronal rate that has been filtered by the PSP. The PSP is typically assumed to integrate to 1 so that $\int_0^\infty \varepsilon(s) ds = 1$.

Since convolution in the temporal domain is multiplication in the frequency domain, neuronal output that has been filtered by a PSP kernel, as defined in Eq. (8), can be expressed using frequency variables by employing the Fourier transform from Eq. (7) to give

$$(f_i^B \star \varepsilon) = \frac{1}{T} \sum_k F_i^B(k) E(k) \exp\left(2\pi i t \frac{k}{T}\right), \quad (9)$$

where $E(k)$ denotes the PSP in the frequency domain at frequency k . Note that since the temporal signals are real, the imaginary frequency components of the PSP filter are conjugate symmetric around 0.

Relaxing the assumption of homogeneous propagation and denoting by $(f_i^{B(\Delta)} \star \varepsilon)$ the rate for neuron i that is a function of both the synapse response kernel and propagation delay, the expressions for neuronal spiking rates in layers B and C as a function of input become

$$(f_i^{B(\Delta)} \star \varepsilon)(t) = R_a^B + \sum_m w_{mi}^{AB} f_m^A(t - \Delta_{mi}^{AB}) \star \varepsilon(t), \quad (10a)$$

$$(f_p^{C(\Delta)} \star \varepsilon)(t) = R_a^C + \sum_i w_{ip}^{BC} (f_i^{B(\Delta)} \star \varepsilon)(t - \Delta_{ip}^{BC}) \star \varepsilon(t). \quad (10b)$$

For simplicity, we suppose that neurons in all layers have the same PSP. However, it is straightforward to incorporate layer-specific PSP functions.

By the linearity of the Fourier transform, Eq. (7), rate can be written as a sum of the input spectral variates. For unitary weights from layer $A \rightarrow B$ and letting $k' = \frac{k}{T}$ for readability, the neuronal activity model that incorporates propagation delay in Eq. (10) can be written as

$$\begin{aligned} (f_i^{B(\Delta)} \star \varepsilon) &= \frac{1}{T} \sum_k \exp(2\pi i t k') \sum_m F_m^A(k) E(k) \exp(-2\pi i \Delta_{mi} k') \\ &= \frac{1}{T} \sum_k \exp(2\pi i t k') E(k) \sum_m F_m^A(k) \exp(-2\pi i \Delta_{mi} k'). \end{aligned} \quad (11)$$

2.3 Neural learning in Linsker's network

2.3.1 Covariance of neural activity

Linsker (1986a) showed that spatial structure in synaptic connections between layers creates temporal covariance in neural activity between cells in layer B onwards. A Gaussian synaptic connection density ensures that layer B neurons situated nearer to each other in the lamina have more layer A connections in common and, consequently, the neural activity of these neurons is more correlated. Layer B neurons are the presynaptic inputs to layer C neurons, also connected with a Gaussian density, parameterized by a unique connectivity radius, $(\sigma^{BC})^2$. The layer B neurons located radially closer to the postsynaptic neuron in layer C will have more nearby neighbors that are also connected to the postsynaptic layer C neuron and, being located near each other, will have more layer A connections in common and so will be more temporally correlated. Thus, a spatial structure in temporal covariance is created. Linsker (1986a) demonstrated that the resulting structure in temporal covariance can generate the emergence of receptive field structure in deeper layers via Hebbian learning, showing the creation of spatial opponent cells in layer C and orientation selective cells in layers deeper in the hierarchy.

Since learning is driven by the covariance of presynaptic neural activity (Kempster et al., 1999a), we derive an expression for covariance between layer B neurons, as given by Linsker (1986a). Initially, we consider learning in an ideal network, such as Linsker (1986a) employed, in which there is uniform propagation delay across all neurons and an implied delta function for the postsynaptic response.

Using the expression for the expected number of shared connections between layer B neurons in Eq. (3), the covariance is given by (see Appendix C)

$$\text{cov}(f_i^B, f_j^B) = \frac{(N^{AB})^2 (\lambda^A)^2}{2\pi(\sigma^{AB})^2} \exp\left(-\frac{d^2}{2(\sigma^{AB})^2}\right). \quad (12)$$

This expression for covariance between layer B neurons is pivotal in determining the final synaptic structure for a stable network (Linsker, 1986a).

Since instantaneous covariance is equivalent to the cross-correlation of zero-meaned variates at lag 0 (see Appendix D for details), we can use Eq. (7) to express covariance between two layer B neurons as

$$\begin{aligned} \text{cov}(f_i^B, f_j^B) &= \frac{1}{T^2} \sum_k (F_i^B(k))^* F_j^B(k) \exp\left(2\pi i 0 \frac{k}{T}\right) \\ &= \frac{1}{T^2} \sum_k (F_i^B(k))^* F_j^B(k). \end{aligned} \quad (13)$$

In the following, when considering neural learning of synapses between layers B and C , it is assumed that synapses between layers A and B have already evolved to maturity such that all synapses are excitatory with unity weight (see Linsker (1986a) for conditions required for this to occur). Therefore, we will consider the plasticity of B to C connections in this work.

2.3.2 Learning equation

Synaptic plasticity occurs adiabatically when compared with neuronal dynamics, being the result of many incremental changes in synapse strength. Furthermore, each neuron within a layer has identical spatial connectivity and firing rate statistics. Consequently, the system can be considered ergodic. This is significant because it enables statistics such as covariance in neuronal firing rate to be evaluated either by taking an ensemble average or a temporal average over a trial or epoch.

Linsker (1986a) assumed that a synapse between two neurons was potentiated if the product of the pre- and post-synaptic neuronal activity was above average, indicating that their activity was positively covaried, and vice-versa. For example,

consider a presynaptic neuron, i , in layer B , and a postsynaptic neuron, p , in layer C , so that

$$\begin{aligned}
\Delta w_{ip}^{BC} &\propto \text{cov} \left(f_i^B - \bar{f}^B, f_p^C - \bar{f}^C \right) \\
&= \text{cov} \left(f_i^B - \bar{f}^B, R_a^C + \sum_j w_{jp}^{BC} f_j^B - \bar{f}^C \right) \\
&= \text{cov} \left(f_i^B - \bar{f}^B, R_a^C + \sum_j w_{jp}^{BC} f_j^B - \left(R_a^C + \sum_j w_{jp}^{BC} \bar{f}^B \right) \right) \\
&= \sum_j \text{cov} \left(f_i^B - \bar{f}^B, w_{jp}^{BC} (f_j^B - \bar{f}^B) \right). \tag{14}
\end{aligned}$$

Consequently, synaptic weight change between a presynaptic neuron, i , in layer B and a postsynaptic neuron, p , in layer C is proportional to the sum of the presynaptic neuron's covariance with all other presynaptic neurons in layer B that input to p .

We can take advantage of the slow change in synaptic weights and the ergodicity of the system by taking an ensemble average of weights across the lamina. The learning equations for synaptic weights can then be expressed as first-order linear differential equations (Linsker, 1986a),

$$\dot{w}_{mi}^{AB} \triangleq \eta \langle (\Delta w_{mi}^{AB}) \rangle = \eta \left(k_1^{AB} + \frac{1}{N^{AB}} \sum w_{ni}^{AB} (Q(f_n^A, f_m^A) + k_2^{AB}) \right), \quad w_{\min}^{AB} \leq w_{mi}^{AB} \leq w_{\max}^{AB}, \tag{15a}$$

$$\dot{w}_{ip}^{BC} \triangleq \eta \langle (\Delta w_{ip}^{BC}) \rangle = \eta \left(k_1^{BC} + \frac{1}{N^{BC}} \sum w_{jp}^{BC} (Q(f_j^B, f_i^B) + k_2^{BC}) \right), \quad w_{\min}^{BC} \leq w_{ip}^{BC} \leq w_{\max}^{BC}, \tag{15b}$$

where $\eta \ll 1$ is the learning rate, chosen to be sufficiently small so that the weights are quasi-constant on the timescale of neuronal dynamics, w_{ni}^{AB} depicts the weight of the synapse connecting presynaptic neuron, n , in layer A to postsynaptic neuron, i , in layer B , and, similarly, w_{jp}^{BC} depicts the weight of the synapse connecting presynaptic neuron, j , in layer B to postsynaptic neuron, p , in layer C . The parameters, k_1^{AB} , k_2^{AB} , and k_1^{BC} , k_2^{BC} , are learning constants that are homogeneous across all synapses connecting two neural populations. $Q(f_n^A, f_m^A)$ and $Q(f_j^B, f_i^B)$ denote the expected covariance in neural activity between neurons n and m in layer A and neurons i and j in layer B , respectively. The definition for each follows the same structure that, for example, for layer B covariance, is $Q(f_j^B, f_i^B) = f_0^{-2} \langle f_j^B - \bar{f}^B \rangle \langle f_i^B - \bar{f}^B \rangle$, where $\langle \rangle$ denotes an ensemble average, f_i^B is the rate of activity of neuron i in layer B , \bar{f}^B is the temporal average of layer B spiking rates in an ergodic system, and f_0^2 is a scaling factor to normalize the covariance matrix, Q . From the expected value of covariance in Eq. (12) it can be seen that to normalize the covariance requires that

$$\begin{aligned}
Q(f_j^B, f_i^B) &= f_0^{-2} \text{cov} (f_i^B, f_j^B) \\
&= \exp \left(-\frac{d^2}{2(\sigma^{AB})^2} \right) \in [0, 1], \tag{16}
\end{aligned}$$

such that

$$f_0^2 = \frac{2\pi(\sigma^{AB})^2}{(N^{AB})^2 (\lambda^A)^2}. \tag{17}$$

Inspection of the weight Eqs. (15a) and (15b) shows that k_1 and k_2 do not depend on input and, therefore, do not drive learning but rather regulate overall activity and determine homeostasis. Without the dependence of the learning equation on input covariance, all weights would evolve to either the upper or lower bound because no presynaptic neuron would be more competitive than another and thus all neurons would change equally.

The weight bounds, $w_{\min} \leq w \leq w_{\max}$, are determined by the proportion of excitatory to inhibitory neurons (Linsker, 1986a). Linsker (1986a) showed that, for a linear network such as this, having a fraction, w_{\max} , of excitatory synapses with limits of 0 and 1, and a fraction, $w_{\min} = 1 - w_{\max}$, of inhibitory synapses with limits of -1 and 0, is equivalent to all synapses having limits of w_{\min} and w_{\max} .

In this work, the term receptive field is considered to refer to an inter-layer receptive field. That is, rather than being defined by stimulus space, it is defined by a cortical neuron's input synaptic weight structure. The receptive field learned by a neuron

is described by the set of synaptic weights from its presynaptic neurons after the system has converged to equilibrium. For neuron i in layer B , the set of presynaptic neurons can be described by $\{m \mid m \text{ has a synaptic connection to } i\}$. Denote by $(w_{mi}^{AB})_*$ the fixed point for the synapse weight from neuron m in layer A to neuron i in layer B . The fixed point is assumed to be reached once all synapse weights, or all but one, are no longer changing (Linsker, 1986a). The set of fixed point weights describe the receptive field learned by neuron i . If a synapse has a weight of 0 then it is not considered to be part of the receptive field.

As in Linsker (1986a), the parameters for the layer A to B connection are chosen such that the weights are unstable and all, or all but one, reach the upper bound, w_{\max}^{AB} . In this way, correlations in the neural activity of layer B cells emerge from spatial structure in the presynaptic input from layer A , rather than structure in the connection weights.

The network governed by learning Eq. (15b) is linear up to the thresholds imposed by the weight bounds. Consequently, derivation of the eigenfunctions for the learning equation will identify the independent components that contribute to the learned structure of a layer C receptive field. Crucially, since the system is unstable (Linsker, 1986a), the eigenfunction with the leading eigenvalue will typically dominate the emerging structure until the weight bounds are reached. We employ the assumption introduced by MacKay and Miller (1990) that states that the structure of the receptive field does not change significantly once all synapses have reached their bounds.

To characterize learning in terms of the eigenfunctions, we employ the continuous limit of neuron position. In the limit, the probability of a synaptic connection existing between a neuron in the presynaptic layer with a neuron in the postsynaptic layer, detailed in Eq. (2), becomes an expression of synapse density. The synaptic weight between layer B neuron i at polar position (r, θ) and layer C neuron p at position $(0,0)$ can be represented by the average strength of a synapse at position (r, θ) , given by Eq. (16).

The system is circularly symmetric so, without loss of generality, we find eigenfunctions for the synaptic weight of an arbitrary neuron in layer B at position (r, θ) connected to a layer C cell positioned at the center of the lamina, $(0,0)$. Owing to the assumption that propagation delay of spikes from layer B to layer C is homogeneous, being dominated by interlaminar distance, the covariance term that drives the structure is a function of radial distance only (Eq. (16)). Consequently, the eigenfunction equation can be written in two dimensions. Using polar coordinates and taking the continuous limit of Eq. (15b), we wish to find the eigenfunctions of

$$w(r, \theta) = A \int_0^\infty d\tilde{r} \tilde{r} \int_0^{2\pi} d\tilde{\theta} \left(\exp\left(-\frac{r^2 + \tilde{r}^2 - 2r\tilde{r}\cos(\theta - \tilde{\theta})}{2(\sigma^{AB})^2}\right) + k_2^{BC} \right) \exp\left(-\frac{\tilde{r}^2 + r^2}{(\sigma^{BC})^2}\right) w(\tilde{r}, \tilde{\theta}), \quad (18)$$

where $w()$ is the continuous time approximation to w and neuron i in layer B is denoted by its position vector, (r, θ) , while the position of neuron j in layer B is given by $(\tilde{r}, \tilde{\theta})$, with neural index subscripts omitted for readability. The coefficient A is $A = \eta (\pi(\sigma^{AB})^2)^{-2}$, arising from Eq. (1).

3 Results

We first provide an eigenfunction solution of the learning equation in Eq. (18). Initially, we solve a simplified learning equation, in which the homeostatic constants, k_1 and k_2 , are set to 0. A perturbation analysis is used to extend this solution to the learning equation with non-zero homeostatic constants.

An expression for covariance between layer B neurons is calculated for the case in which an arbitrary PSP is included in the neuron model, Eq. (8), and then for the case in which a PSP and three-dimensional propagation delay is incorporated into the neuron model, Eq. (10). Finally, since we assume that the plasticity mechanism is initiated near the site of a layer C cell body, covariance is calculated for the neural activity of two presynaptic layer B cells, at the time this activity is received by the postsynaptic neuron in layer C .

We calculate the expected size of a layer C neuron's receptive field when Linsker's (1986a) neuron model is employed, Eq. (6); i.e. when there is an implicit delta function model of a PSP and inter-lamina delay is implicitly assumed to dominate propagation delay sufficiently such that radial propagation delay is negligible.

Using the expressions derived for covariance between layer B neurons when activity is filtered by an arbitrary PSP, we calculate receptive field size for a layer C neuron. Finally, we analytically determine the receptive field size of a layer C cell in the presence of three-dimensional propagation delay.

Following the examination of changes in receptive field size in response to propagation delay and PSP, we determine expressions for the eigenfunctions of the learning system when employing a generalized neuron model that incorporates both propagation delay and arbitrary PSP. Initially, we solve a simplified system with the homeostatic constants set to zero. Then we examine the full learning system with non-zero homeostatic constants.

3.1 Eigenfunctions of the simplified learning equation

Initially, we consider a simplified system by assuming that $k_1^{BC} = k_2^{BC} = 0$. This enables identification of the eigenfunctions driving the structure of the receptive field. The simplified continuous learning equation is

$$w(r, \theta) = A \int_0^\infty d\tilde{r} \tilde{r} \int_0^{2\pi} d\tilde{\theta} \exp\left(-\frac{r^2 + \tilde{r}^2 - 2r\tilde{r}\cos(\theta - \tilde{\theta})}{2(\sigma^{AB})^2}\right) \exp\left(-\frac{\tilde{r}^2 + r^2}{(\sigma^{BC})^2}\right) w(\tilde{r}, \tilde{\theta}), \quad (19)$$

where the coefficient, A , contains the constant terms from the synaptic connection probability (Eq. (1)), such that

$$A = \left(\frac{1}{\pi(\sigma^{AB})^2}\right)^2. \quad (20)$$

MacKay and Miller (1990) provided the first six eigenfunctions to this simplified learning equation. However, a general expression for the eigenfunctions was not provided and a derivation of the eigenfunctions was not included. Wimbauer et al. (1998) provided analytical expressions for the Cartesian eigenfunctions of Linsker (1986a) network, generalized to incorporate recurrent cortical connections. The eigenfunctions for the full learning equation, with non-zero k_2^{BC} , were empirically determined. We derive a general analytical expression for the eigenfunctions of the simplified learning equation in polar format and extend these results via a perturbation analysis to provide an expression for the eigenfunctions of the full learning equation.

The eigenvectors of Eq. (19) have been derived in both polar and Cartesian coordinates in (Davey et al., 2018). The polar eigenfunctions are

$$\mathbf{v}_{l,n}(r, \theta) = N_{ln} \tilde{r}^{l-n} \exp\left(-\frac{r^2}{2C}\right) L_n^{l-n}\left(\frac{r^2}{C}\right) \exp(i(l-n)\theta), \quad (21)$$

where l and n are indices that determine the order of the eigenfunction, such that $l = 0, 1, \dots$, $n = 0, 1, \dots, l$, and the eigenfunction order is given by $n + l$. The degeneracy for order $(n + l)$ is $(n + l + 1)$. $L_n^{l-n}()$ is an associated Laguerre polynomial. The value of C is (Davey et al., 2018)

$$C = \frac{(\sigma^{BC})^2}{2\sqrt{1 + \frac{2(\sigma^{BC})^2}{(\sigma^{AB})^2}}}, \quad (22)$$

and the normalization factor is defined by

$$N_{ln} = \begin{cases} \sqrt{\frac{2n!}{\pi l! C^{l-n+1} (\sigma^{AB})^2}}, & l = n \\ \sqrt{\frac{n!}{\pi l! C^{l-n+1} (\sigma^{AB})^2}}, & \text{otherwise,} \end{cases} \quad (23)$$

where the factor of 2 difference occurs for the case $l = n$, because the integral for the angular component is over $\cos(0\theta)$, a constant.

Eigenfunction $\mathbf{v}_{l,n}(r, \theta)$ has an eigenvalue of

$$\lambda_{l,n} = 2\pi A \left(\frac{C(\sigma^{BC})^2}{C((\sigma^{AB})^2 + (\sigma^{BC})^2) + (\sigma^{BC})^2} \right)^{l+n+1}. \quad (24)$$

Fig. 2 shows the eigenfunctions for the first five orders, such that $n + l = 0, \dots, 4$. From the figure, it can be seen that a radially symmetric eigenfunction, with all weights at the upper threshold, has the leading eigenvalue.

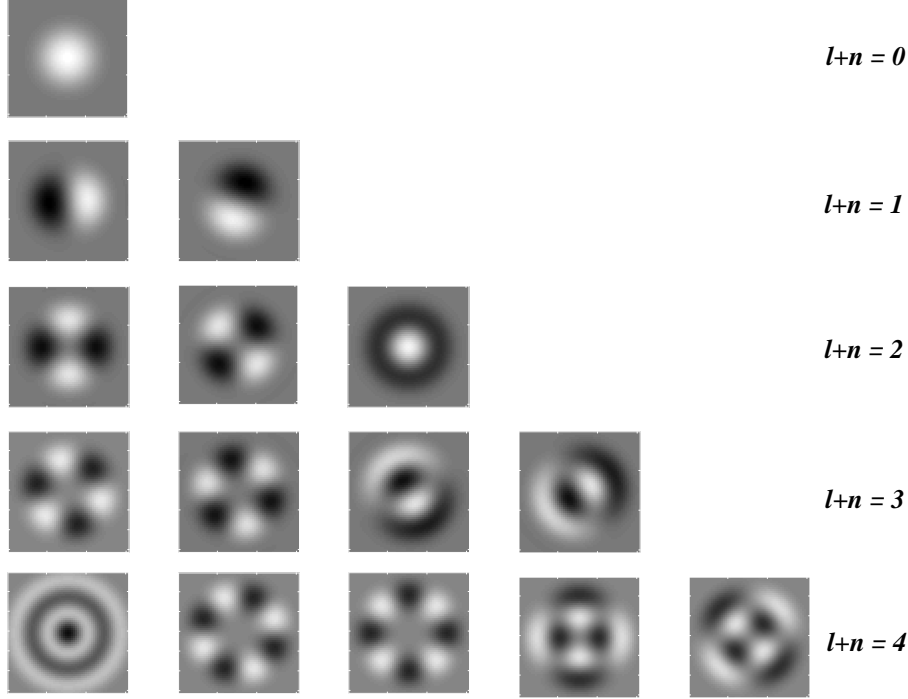


Figure 2: The first five eigenfunctions of Eq. (15b) in order of decreasing eigenvalue, so that $n + l = 0$ has the largest eigenvalue, while $n + l = 4$ has the smallest eigenvalue of those shown in this figure. The figure shows the strength of synapses in B for each eigenfunction of the learning equation for a postsynaptic neuron in C . This figure was generated with synaptic connectivity values of $\sigma^{AB} = 10$ and $\sigma^{BC} = 20$.

3.2 Eigenfunctions of the full learning equation

While covariance between the activity of layer B input neurons primarily drives the structure of the layer C cell, the k_1 and k_2 terms control the homeostatic equilibrium. MacKay and Miller (1990) empirically showed that the choice of k_2^{BC} can change the structure of the dominant eigenfunction and hence the resultant receptive field of a layer C cell. As Fig. 2 shows, for the simplified system, the leading eigenvalue has all synapses at the upper or the lower, bound. For a negative value of k_2^{BC} , homeostasis can only be reached if some of the synapses are negative and so this eigenfunction changes. To examine the impact of the learning constant, we find an analytical expression for the eigenfunctions of the full learning equation, Eq. (18), by conducting a perturbation analysis on the simplified learning equation, Eq. (19).

If the simplified learning Eq. (19) is denoted by $H^0(\mathbf{v}_{l,n}(r, \theta))$ then, from the eigenfunctions derived for the simplified learning equation, we know that

$$\lambda_{l,n} \mathbf{v}_{l,n}(r, \theta) = H^0(\mathbf{v}_{l,n}(r, \theta)). \quad (25)$$

If we perturb the simplified learning equation by adding a small k_2^{BC} , denote the perturbed system by $H^1(\cdot)$, and the eigenfunctions of the perturbed system by $\mathbf{v}_{l,n}^1(r, \theta)$, so that

$$H^1(\mathbf{v}_{l,n}^1(r, \theta)) = A \int_0^\infty d\tilde{r} \tilde{r} \int_0^{2\pi} d\tilde{\theta} \left(\exp\left(-\frac{r^2 + \tilde{r}^2 - 2r\tilde{r}\cos(\theta - \tilde{\theta})}{2(\sigma^{AB})^2}\right) + k_2^{BC} \right) \exp\left(-\frac{\tilde{r}^2 + r^2}{(\sigma^{BC})^2}\right) w(\tilde{r}, \tilde{\theta}), \quad (26)$$

so that the perturbation on the integral operator is

$$\delta H^1(\mathbf{v}_{l,n}(r, \theta)) = A \int_0^\infty d\tilde{r} \tilde{r} \int_0^{2\pi} d\tilde{\theta} k_2^{BC} \exp\left(-\frac{\tilde{r}^2 + r^2}{(\sigma^{BC})^2}\right) w(\tilde{r}, \tilde{\theta}). \quad (27)$$

We require the new eigenfunctions to be similar to the eigenfunctions of the simplified learning equation, plus a small perturbation, so that the first order corrections to the eigenfunctions and eigenvalues can be defined as

$$\mathbf{v}_{l,n}^1(r, \theta) = \mathbf{v}_{l,n}(r, \theta) + \delta \mathbf{v}_{l,n}^1(r, \theta), \quad \lambda_{l,n}^1 = \lambda_{l,n} \mathbf{v}_{l,n}(r, \theta) + \delta \lambda_{l,n}^1. \quad (28)$$

For non-degenerate eigenfunctions, the first-order corrections can be determined by (Kato, 1995)

$$\delta \mathbf{v}_{l,n}^1(r, \theta) = \sum_{l+n \neq m+p} \frac{\int_{-\infty}^{\infty} dr r \int_0^{2\pi} d\theta (\mathbf{v}_{l,n}(r, \theta))^* \delta H^1(\mathbf{v}_{l,n}(r, \theta)) \mathbf{v}_{m,p}(r, \theta)}{\lambda_{l,n} - \lambda_{m,p}}, \quad (29)$$

for non-degenerate eigenfunctions, i.e. $l+n \neq m+p$. For degenerate eigenfunctions, the denominator of Eq. (29) is equal to zero. However, if $W_{l,n}^{m,p} = \sum \int_{-\infty}^{\infty} dr r \int_0^{2\pi} d\theta (\mathbf{v}_{l,n}(r, \theta))^* H^1(\mathbf{v}_{l,n}(r, \theta)) \mathbf{v}_{m,p}(r, \theta)$ then the first order correction of degenerate eigenfunctions of order $l+n$, can be found as the eigenfunctions of the $(l+n) \times (l+n)$ matrix of $W_{l,n}^{m,p}$ coefficients. Given that the degenerate eigenfunctions of order $l+n$ either have angular terms with different frequencies or are out of phase by 90° , the off-diagonal terms of this matrix are zero. Hence, the eigenvectors of this matrix are simply the diagonal terms of $W_{l,n}^{m,p}$. Consequently, it is only necessary to evaluate the diagonal terms. The same logic applies to the non-degenerate eigenfunctions, meaning that it is only necessary to evaluate the diagonal terms, which are denoted by the single index pair, $W_{l,n}$, and can be evaluated as

$$\begin{aligned} W_{l,n} &= 2\pi A N_{ln}^2 \int_0^{\infty} d\tilde{r} \tilde{r} r^{2(l-n)} \exp\left(-\frac{r^2}{C}\right) \exp\left(-\frac{\tilde{r}^2 + r^2}{(\sigma^{BC})^2}\right) \left[L_n^{l-n}\left(\frac{r^2}{C}\right) \right]^2 \\ &= \pi A N_{ln}^2 C^{l+n+1} \exp\left(-\frac{r^2}{(\sigma^{BC})^2}\right) \int_0^{\infty} dz z^{l-n} \exp(-\alpha z) \left[L_n^{l-n}(z) \right]^2, \end{aligned} \quad (30)$$

where $\alpha = \frac{(\sigma^{BC})^2 + C}{(\sigma^{BC})^2}$. This integral on the right-hand side can be evaluated as (Gradshteyn and Ryzhik, 2007)

$$\int_0^{\infty} e^{-bx} x^a L_n^a(x) L_m^a(x) dx = \frac{\Gamma(m+n+a+1)(b-1)^{n+m}}{m!n!b^{m+n+a+1}} {}_2F_1\left(-m, -n; -m-n-a; \frac{b(b-2)}{(b-1)^2}\right),$$

where ${}_2F_1(\cdot)$ is the hypergeometric function and, hence,

$$W_{l,n} = \pi C^{l-n+1} k_2^{BC} N_{ln}^2 \frac{\Gamma(l+n+1)(\alpha-1)^{2n}}{n!^2 \alpha^{l+n+1}} {}_2F_1\left(-n, n; l-n; \frac{\alpha(\alpha-2)}{(\alpha-1)^2}\right). \quad (31)$$

Since only the diagonal terms are non-zero, the shape of the perturbed eigenfunctions remains the same as those for the simplified learning equation, given in Eq. (21), but the eigenvalues change according to

$$\lambda_{l,n}^1 = \lambda_{l,n} + W_{l,n}. \quad (32)$$

For positive k_2 , the perturbation on the eigenvalues is positive and monotonically decreasing. Consequently, the order of the eigenvalues remains the same. For negative k_2 , the perturbation on the eigenvalues is monotonically decreasing. Since these perturbations are being added to the original eigenvalues, which are large and positive for the low-order eigenfunctions, the result can be a change in the dominant eigenfunction. This result supports the empirical findings by MacKay and Miller (1990) that showed the emergence of a spatial opponent cell in C , where $l+n=0$ for small values of k_2 , and bilobed cells with $l+n=1$ for larger values of k_2 .

3.3 Neural learning with propagation delay

3.3.1 Covariance of neural activity with propagation delay

In the network Linsker studied, there was equal transmission delay between neurons and rate changes were instantaneous, implying that the postsynaptic response function (PSP) of cells was implicitly a delta function. In this study we develop a framework for incorporating delay and a non-trivial PSP function, and derive expressions for the covariance between layer B neurons and neural learning in synapses connecting layers B and C . This is a first step towards understanding neural learning

with temporal dynamics, such as processing moving images. We assess the impact of delay and PSP function on the covariance of neurons and, hence, on the development of structure in a Linsker-type network. In order to understand how various parameters, such as propagation delay, impact the evolution of spatial opponent cells, it is necessary to derive equations for the expected size of a cell's receptive field and the learning time constant.

Using the expression for covariance between layer B , neurons we then determine the expected receptive field size of a layer C neuron as a function of both temporal and spatial parameters. In this way, we determine the impact of propagation delay on the emerging structure of the layer C cells.

3.3.1.1 Network incorporating a general post-synaptic response To determine an expression for covariance between neurons whose activity has been filtered by a PSP kernel, Eq. (8), we extend the frequency domain expression for covariance between Poisson neurons with an implicit delta model of the PSP, Eq. (13), to obtain

$$\begin{aligned}
\text{cov}((f_i^B \star \varepsilon), (f_j^B \star \varepsilon)) &= \frac{1}{T^2} \sum_k (F_i^B)^* F_j^B (E(k))^* E(k) \\
&= \frac{1}{T^2} \text{E} \left[(F_i^B)^* F_j^B \right] \sum_k (E(k))^* E(k) \\
&= \text{cov}((f_i^B \star \varepsilon), (f_j^B \star \varepsilon)) \frac{\sum_k (E(k))^* E(k)}{T} \\
&= \kappa^\varepsilon \text{cov}((f_i^B \star \varepsilon), (f_j^B \star \varepsilon)). \tag{33}
\end{aligned}$$

where the second last line follows from Eq. (7) and we have introduced κ^ε such that

$$\kappa^\varepsilon = \frac{\sum_k (E(k))^* E(k)}{T} \leq 1. \tag{34}$$

Note that we have assumed that the PSP function is identical for neurons across all layers. However, it is straightforward to relax this assumption and utilize specific PSP functions for each neuron population.

3.3.1.2 Network incorporating propagation delay and a general postsynaptic response We relaxed the assumption of homogeneous propagation delay for spikes from presynaptic neurons by incorporating a distance-dependent delay in the neuron model, Eq. (10). An expression for covariance between layer B neurons can be obtained by again using the frequency domain expression for covariance in Eq. (13) with respect to the spectral variates for the neuron model incorporating delay, Eq. (11),

$$\text{cov}((f_i^{B(\Delta)} \star \varepsilon), (f_j^{B(\Delta)} \star \varepsilon)) = \frac{1}{T^2} \sum_k \left(E(k) \sum_m F_m^A(k) \exp\left(-2\pi i \Delta_{mi} \frac{k}{T}\right) \right)^* E(k) \sum_n F_n^A(k) \exp\left(-2\pi i \Delta_{ni} \frac{k}{T}\right). \tag{35}$$

Given that the delay variables, Δ_{mi} and Δ_{ni} , are statistically independent of the layer A rate values, F_m^A and F_n^A , respectively, the inner sum terms can be separated to give

$$\begin{aligned}
\text{cov}((f_i^{B(\Delta)} \star \varepsilon), (f_j^{B(\Delta)} \star \varepsilon)) &= \frac{1}{T^2} \sum_k (E(k))^* E(k) \left(\text{E} \left[\exp\left(-2\pi i \Delta_{mi} \frac{k}{T}\right) \right] \right)^* \text{E} \left[\exp\left(-2\pi i \Delta_{ni} \frac{k}{T}\right) \right] \left(\sum_m F_m^A(k) \right)^* \sum_n F_n^A(k) \\
&= \frac{1}{T^2} \sum_k (E(k))^* E(k) \left(\text{E} \left[\exp\left(-2\pi i \Delta_{mi} \frac{k}{T}\right) \right] \right)^* \text{E} \left[\exp\left(-2\pi i \Delta_{ni} \frac{k}{T}\right) \right] (F_i^B(k))^* F_j^B(k). \tag{36}
\end{aligned}$$

If the expected value of delay is denoted by $D^{AB}(k) = \text{E} \left[\exp\left(-2\pi i \Delta \frac{k}{T}\right) \right]$ then covariance between layer B neurons in the presence of delay and an PSP can be expressed as

$$\text{cov}((f_i^{B(\Delta)} \star \varepsilon), (f_j^{B(\Delta)} \star \varepsilon)) = \frac{1}{T^2} \sum_k (E(k))^* E(k) (D^{AB}(k))^* D^{AB}(k) (F_i^B(k))^* F_j^B(k). \tag{37}$$

Derivation of the expected value of delay in the frequency domain is given in Appendix E. The derivation integrates the Fourier transform of propagation delay, $\exp(-2\pi i \Delta_{mi} \frac{k}{T})$, between each presynaptic neuron, m , in layer B and the postsynaptic neuron, i , in layer C over the presynaptic layer, weighted by the probability of the presynaptic neuron having a connection to the postsynaptic neuron, Eq. (4). Note that delay is determined from the three-dimensional distance between the pre- and post-synaptic neurons, comprised of the radial distance, d_{mi}^B , the interlaminar distance, d^{AB} , and the speed of propagation, v , Eq. (5) (see Fig. 1 for schematic). Given that neurons that are the same distance from the postsynaptic neuron will have the same propagation delay and the same probability of connection, the integration is done in concentric rings of increasing distance from the postsynaptic neuron. Since the integral is over a complex domain, it is solved using contour integration,

$$\begin{aligned}
D^{AB}(k) &= \mathbb{E} \left[\exp \left(-2\pi i \Delta \frac{k}{T} \right) \right] \\
&= \exp \left(-2\pi i \frac{k}{T} \frac{d^{AB} \mu}{v} \right) \\
&\quad - \pi^{3/2} \frac{k}{T} \frac{\sigma^{AB} \mu}{v} \exp \left(\frac{(d^{AB})^2}{(\sigma^{AB})^2} \right) \exp \left(- \left(\pi \frac{k}{T} \frac{\sigma^{AB} \mu}{v} \right)^2 \right) \left(\text{ierfc} \left(\frac{d^{AB}}{\sigma^{AB}} \right) + \text{erf} \left(\frac{d^{AB}}{\sigma^{AB}} + i\pi \frac{k}{T} \frac{\sigma^{AB} \mu}{v} \right) - \text{erf} \left(\frac{d^{AB}}{\sigma^{AB}} \right) \right).
\end{aligned} \tag{38}$$

The expression for the mean value of delay in the frequency domain is essentially a function of two parameters,

$$\tau_l = \frac{d^{AB} \mu}{v} ([\tau_l] = s), \quad \tau_r = \frac{\sigma^{AB} \mu}{v} ([\tau_r] = s), \tag{39}$$

where τ_l depicts the propagation time between layers and τ_r represents the radial propagation time within the lamina. Consequently, mean delay in frequency can be written as

$$D^{AB}(k) = \exp \left(-2\pi i \frac{k}{T} \tau_l \right) - \pi^{3/2} \frac{k}{T} \tau_r \exp \left(\left(\frac{\tau_l}{\tau_r} \right)^2 \right) \exp \left(- \left(\pi \frac{k}{T} \tau_r \right)^2 \right) \left(\text{ierfc} \left(\frac{\tau_l}{\tau_r} \right) + \text{erf} \left(\frac{\tau_l}{\tau_r} + i\pi \frac{k}{T} \tau_r \right) - \text{erf} \left(\frac{\tau_l}{\tau_r} \right) \right). \tag{40}$$

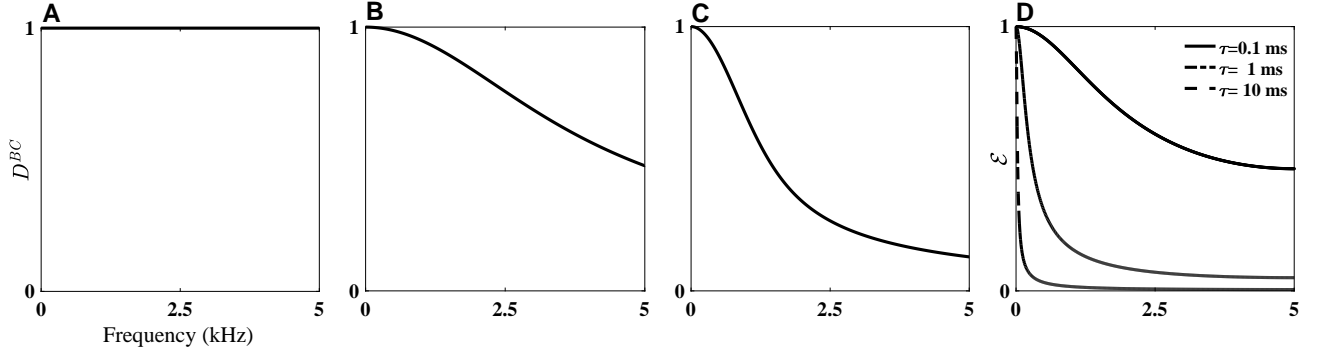


Figure 3: **(A-C)** Magnitude of the expected value of delay Eq. (40), in the frequency domain for different radial propagation delays, τ_r . The x-axis shows frequencies, k' , up to the Nyquist frequency, from 0 to 5 kHz. The y-axis is $D^{AB}(k) \in [0, 1]$. The inter-layer propagation delay was $\tau_l = 500 \mu\text{s}$, derived from velocity, $v = 2 \text{ m/s}$, and neural density, $\mu = 10 \mu\text{m}$. The radial propagation delay was; **(A)** $\tau_r = 50 \mu\text{s}$, **(B)** $\tau_r = 250 \mu\text{s}$, **(C)** $\tau_r = 500 \mu\text{s}$. **(D)** shows the magnitude of an example PSP in the frequency domain, normalized between 0 and 1, to enable comparison with frequencies retained in rate-based neural activity after incorporating the impact of propagation delay. In this example the PSP is modelled with a single parameter, the decay time, τ , such that $\varepsilon \propto \exp(-\frac{t}{\tau})$, so that $E \propto \frac{\tau}{k' \tau + 1}$, and normalized to 1.

Fig. 3 shows the mean delay as a function of different radial propagation velocities, which is determined by the connection radius, the neuron density, and spike propagation velocity, as detailed in Eq. (39). For comparatively small radial propagation delays relative to inter-layer propagation delay (Fig. 3A), the delay of all spikes from the presynaptic layer to a postsynaptic

neuron is approximately equal, and the impact of delay is negligible. As the radial propagation delay increases relative to the inter-layer propagation delay, the propagation time from presynaptic neurons to a postsynaptic neuron can no longer be assumed approximately equal and the spread in arrival times to the postsynaptic neuron attenuates covariance between the layer B postsynaptic neurons (Fig. 3B,C). Example frequency profiles for the PSP are shown in Fig. 3D, in which the PSP is modelled as a single exponential with the decay parameter chosen to reflect the effective membrane time constant, which is shorter than the membrane time constant due to the neuron becoming more leaky as more synaptic channels open (Burkitt et al., 2003). For PSPs with long decay times, the Fourier transform, E , contains only low frequencies, and for inter-lamina distances that dominate radial distances, the propagation delay between layers dominates the radial propagation delay sufficiently that the mean delay in frequency, $D^{AB}(k) \in [0, 1]$, attenuates only the very highest frequencies. Consequently, propagation delay does not destroy frequencies that are present in the neuronal signal.

For the case where radial propagation delay is on the order of inter-laminar propagation delay, high frequency information is increasingly attenuated as covariance from presynaptic neurons becomes increasingly spread in arrival time at the postsynaptic neuron, causing frequencies that are present in the PSP to be decimated.

Finally, the expression for covariance between filtered and delayed input rates is

$$\begin{aligned} \text{cov}\left((f_i^{B(\Delta)} \star \varepsilon), (f_j^{B(\Delta)} \star \varepsilon)\right) &= \frac{1}{T^2} \sum_k (E(k))^* E(k) (D^{AB}(k))^* D^{AB}(k) (F_i^B(k))^* F_j^B(k) \\ &= \text{cov}(f_i^B, f_j^B) \frac{\sum_k (E(k))^* E(k) (D^{AB}(k))^* D^{AB}(k)}{T} \\ &= \kappa_\Delta^{AB} \kappa^\varepsilon \text{cov}(f_i^B, f_j^B), \end{aligned} \quad (41)$$

where κ^ε captures the attenuation induced by the low pass filtering of the PSP, Eq. (34), and κ_Δ^{AB} expresses the attenuation of the signal by propagation delay and is defined by

$$\kappa_\Delta^{AB} = \frac{\sum_k (D^{AB}(k))^* D^{AB}(k)}{T} \leq 1. \quad (42)$$

3.3.2 Learning equation with propagation delay

Thus far, we have derived the covariance between the neural activity of layer B neurons. However, when these neurons propagate spikes to a postsynaptic layer C neuron, there will be a delay as the signal propagates from layer B to layer C , where arrival at the postsynaptic neuron will cause the signal to be further filtered by the postsynaptic cell's PSP function. To evaluate the impact of this, it is necessary to consider the origin of the learning rule in Eq. (15b), outlined in Eq. (14), in the context of the presynaptic output being delayed before arriving at the synapse where learning occurs, and the postsynaptic neural activity being filtered again at the layer C site. Using the model for layer C neural activity given in Eq. (10b), and assuming that the plasticity process of synapse weight change is initiated near the cell body of the post-synaptic neuron, the learning equation becomes,

$$w_{ip}^{BC} = \eta \left(k_1^{BC} + \frac{1}{N^{BC}} \sum w_{jp}^{BC} \left(Q \left((f_j^{B(\Delta)} \star \varepsilon) (t - \Delta_{jp}^{BC}), (f_i^{B(\Delta)} \star \varepsilon) (t - \Delta_{ip}^{BC}) \star \varepsilon(t) \right) + k_2^{BC} \right) \right), \quad (43)$$

where Q is the normalized form of covariance between layer B neurons.

To evaluate this covariance in the presence of propagation delay and arbitrary PSP, we can use the framework established in Section 3.3.1.2. Application of the result in Eq. (41) to calculate covariance between layer B output, and layer C input, and using $D^{AB}(k)$ from Eq. (38), we obtain

$$\begin{aligned} &\text{cov}\left((f_j^{B(\Delta)} \star \varepsilon) (t - \Delta_{jp}^{BC}), (f_i^{B(\Delta)} \star \varepsilon) (t - \Delta_{ip}^{BC}) \star \varepsilon(t)\right) \\ &= \frac{1}{T^2} \sum_k \left(E(k) \exp\left(-2\pi i \Delta_{jp}^{BC} \frac{k}{T}\right) \sum_n F_n^A(k) \exp\left(-2\pi i \Delta_{nj}^{AB} \frac{k}{T}\right) \right)^* E(k)^2 \exp\left(-2\pi i \Delta_{ip}^{BC} \frac{k}{T}\right) \sum_m F_m^A(k) \exp\left(-2\pi i \Delta_{mi}^{AB} \frac{k}{T}\right) \\ &= \frac{1}{T^2} \sum_k (E(k))^* E(k)^2 (D^{AB}(k))^* D^{AB}(k) \exp\left(-2\pi i \frac{k}{T} (\Delta_{ip}^{BC} - \Delta_{jp}^{BC})\right) (F_i^B(k))^* F_j^B(k) \\ &= \text{cov}(f_i^B, f_j^B) \frac{1}{T} \sum_k (E(k))^* E(k)^2 (D^{AB}(k))^* D^{AB}(k) \exp\left(-2\pi i \frac{k}{T} (\Delta_{ip}^{BC} - \Delta_{jp}^{BC})\right). \end{aligned} \quad (44)$$

Note that the result depends on the position of the layer B presynaptic neuron, i , relative to the layer C postsynaptic neuron p , because the output of the postsynaptic neuron in layer C will be delayed by an amount proportional to the distance between them. More precisely, the result depends on the difference in spike arrival time between neuron i and neuron j at the neuron p in layer C , given by $\Delta_{ip}^{BC} - \Delta_{jp}^{BC}$, which itself is a function of the radial distance between i , and j , the interlaminar distance between layers B and C , and the spike propagation velocity, i.e. $\Delta_{ip}^{BC} - \Delta_{jp}^{BC} = \frac{((d_{ip}^B)^2 + (d^{BC})^2)^{\frac{1}{2}} - ((d_{jp}^B)^2 + (d^{BC})^2)^{\frac{1}{2}}}{v}$. If the Fourier transform of the time shift component, $\exp\left(-2\pi i \frac{k}{T} \left(\Delta_{ip}^{BC} - \Delta_{jp}^{BC}\right)\right)$, is independent of the PSP function, $E(k)$, and the mean delay function, $D^{BC}(k)$, then the time shift component can be moved out of the sum. In this event, covariance will be zero, since clearly the mean time shift will evaluate to 0. This is intuitive since, if there is no relationship between the time shift and the PSP filter, all of the covariance will be destroyed. Consequently, to evaluate covariance between the layer B signal on arrival at the post-synaptic neuron in layer C requires a specific form for the PSP.

To evaluate covariance between the inputs of a layer C neuron, we propose a simple one-sided exponential PSP such that $\varepsilon = \tau_\varepsilon^{-1} \exp\left(-\frac{t}{\tau_\varepsilon}\right)$. In this case, we have $(E(k))^* E(k) = \frac{1}{1+(2\pi \frac{k}{T} \tau_\varepsilon)^2}$ and $(E(k))^* E(k) E(k) = \frac{1}{1+(2\pi \frac{k}{T} \tau_\varepsilon)^2} \frac{1}{1+2\pi \frac{k}{T} \tau_\varepsilon}$. Substituting this into Eq. (44) gives

$$\begin{aligned} & \text{cov}\left((f_j^{B(\Delta)} \star \varepsilon)(t - \Delta_{jp}^{BC}), (f_i^{B(\Delta)} \star \varepsilon)(t - \Delta_{ip}^{BC})\right) \\ &= \text{cov}(f_i^B, f_j^B) \frac{1}{T} \sum_k \frac{1}{\left(1 + (2\pi \frac{k}{T} \tau_\varepsilon)^2\right)} \frac{1}{\left(1 + 2\pi \frac{k}{T} \tau_\varepsilon\right)} (D^{AB}(k))^* D^{AB}(k) \exp\left(-2\pi i \frac{k}{T} (\Delta_{ip}^{BC} - \Delta_{jp}^{BC})\right) \\ &= \kappa_\Delta^{AB} \text{cov}(f_i^B, f_j^B) \exp\left(-\frac{|\Delta_{ip}^{BC} - \Delta_{jp}^{BC}|}{\tau_\varepsilon}\right), \end{aligned} \quad (45)$$

for lag-0 covariance. Consequently, neurons that are spaced further apart in the laminar have covariance attenuated to a greater extent as the difference in arrival time of pre-synaptic spikes at the post-synaptic neuron increases with distance. However, the PSP slows down this distance-induced attenuation by spreading the probability of the spike across a period of time, determined by τ_ε .

The rate of change of synaptic weights between layers B and C can then be given as

$$\dot{w}_{ip}^{BC} \triangleq \eta \langle (\Delta w_{ip}) \rangle = \eta \left(k_1^{BC} + \frac{\kappa_\Delta^{AB}}{N^{BC}} \sum w_{jp}^{BC} \left(\exp\left(-\frac{|\Delta_{ip}^{BC} - \Delta_{jp}^{BC}|}{\tau_\varepsilon}\right) Q(f_j^B, f_i^B) + k_2^{BC} \right) \right). \quad (46)$$

3.4 On-center size

For cortical neurons, the term receptive field is assumed to refer to an inter-layer receptive field, defined by a cortical neuron's input synaptic weight structure. We wish to analytically derive an expression for the size of the on-center of a cell's receptive field to determine the impact of propagation delay on the evolution of layer C spatial-opponent cells. To this end, we consider the cell when it has undergone sufficient learning (see the learning equation, Eq. (15b)) such that the weights of all synapses connecting to the layer C cell have diverged to the upper or lower bound. This assumption is valid because the learning equation is unstable, and hence all weights, or all but one, will reach a stable limiting value (see page 7510, Linsker (1986a)).

3.4.1 Linsker's network

To determine the size of a cell's on-center, it is necessary to determine its average synaptic weight. We assume that synaptic weights are independent of covariance between neural output early in the learning process. The mean weight converges during this early stage (Kempton et al., 1999a), and thus from Eq. (15b), we can write

$$\bar{w}^{BC} = \eta \left(k_1^{BC} + \bar{w}^{BC} \left(k_2^{BC} + \overline{Q^{BB}} \right) \right), \quad w_{\min}^{BC} \leq \bar{w}^{BC} \leq w_{\max}^{BC}, \quad (47)$$

where \bar{w}^{BC} denotes the mean weight of synapses between layer B and layer C and $\overline{Q^{BB}}$ is the mean covariance between layer B neural outputs. As noted by Linsker (1986a), for $k_2^{BC} > 0$, the weights are unstable and grow to the bounds. Linsker (1986a)

showed that k_2^{BC} can be derived from first-order firing rate statistics and is positive if the postsynaptic neuron is firing at a rate that is greater than a given constant benchmark rate, and vice-versa. This means that, for the mean weight to be stable, the mean rate of neural firing must be less than this benchmark value.

The fixed point for the mean weight, \bar{w}_*^{BC} , follows immediately,

$$\bar{w}_*^{BC} = \frac{-k_1^{BC}}{k_2^{BC} + Q^{BB}}. \quad (48)$$

To determine the fixed point for the mean weight, we need to calculate the mean covariance between layer B neurons. As in Linsker (1986a), we normalize the temporal covariance between layer B neurons by dividing by input variance and number of input connections (Eqs. (16) and (17)). Consequently, for the case of a delta function PSP and instantaneous propagation delay, the covariance of a neuron with itself is 1. The average covariance between layer B neurons can now be found by integrating covariance over the laminar (see Appendix F for details),

$$\begin{aligned} \overline{Q^{BB}} &= \frac{1}{(\pi(\sigma^{BC})^2)^2} \int_{-\infty}^{\infty} \int_{-\infty}^{\infty} \exp\left(-\frac{|\mathbf{x}^2 - \mathbf{x}'^2|}{2(\sigma^{AB})^2}\right) \exp\left(-\frac{\mathbf{x}^2}{(\sigma^{BC})^2}\right) \exp\left(-\frac{\mathbf{x}'^2}{(\sigma^{BC})^2}\right) d\mathbf{x}' d\mathbf{x} \\ &= \frac{1}{1 + \frac{(\sigma^{BC})^2}{(\sigma^{AB})^2}}. \end{aligned} \quad (49)$$

From Eq. (49), it can be seen that mean covariance between layer B neurons is maximized by either maximizing the connection radius between layers A and B or minimizing the connection radius between layers B and C .

Now it is necessary to calculate the average weight of a layer C synapse with receptive field size of r_{on} . Knowing that synapses within the on-center have reached the upper limiting value of w_{max}^{BC} , while synapses outside of it have reached the lower limiting value of w_{min}^{BC} , we can determine the average synaptic weight by integrating individual synapse weights scaled by the probability of each synapse being connected to the layer C neuron. Implementing the integral in polar coordinates this time, we obtain

$$\begin{aligned} \bar{w}_*^{BC} &= \frac{w_{\text{max}}^{BC}}{\pi(\sigma^{BC})^2} \int_0^{r_{\text{on}}} \int_0^{2\pi} \exp\left(-\frac{\tilde{r}^2}{(\sigma^{BC})^2}\right) d\tilde{r} d\tilde{\theta} - \frac{w_{\text{min}}^{BC}}{\pi(\sigma^{BC})^2} \int_{r_{\text{on}}}^{\infty} \int_0^{2\pi} \exp\left(-\frac{\tilde{r}^2}{(\sigma^{BC})^2}\right) d\tilde{r} d\tilde{\theta} \\ &= w_{\text{max}}^{BC} \left(1 - \exp\left(-\frac{(r_{\text{on}})^2}{(\sigma^{BC})^2}\right)\right) + w_{\text{min}}^{BC} \left(\exp\left(-\frac{(r_{\text{on}})^2}{(\sigma^{BC})^2}\right)\right). \end{aligned} \quad (50)$$

For a lower weight bound of 0 and an upper weight bound of 1, this gives

$$\bar{w}_*^{BC} = 1 - \exp\left(-\frac{(r_{\text{on}})^2}{(\sigma^{BC})^2}\right). \quad (51)$$

Finally, to determine the size of the on-center as a function of covariance, equate the two equations for mean synaptic weight, Eqs. (48) and (50), and rearrange to obtain

$$r_{\text{on}} = \sigma^{BC} \sqrt{\log\left(\frac{k_2^{BC} + \overline{Q^{BB}}}{w_{\text{max}}^{BC} (k_2^{BC} + \overline{Q^{BB}}) + k_1^{BC}}\right)} \quad (52)$$

$$= \sigma^{BC} \sqrt{\log\left(\frac{1}{w_{\text{max}}^{BC} - \bar{w}_*^{BC}}\right)}, \quad (53)$$

where we have used the assumption that $w_{\text{max}}^{BC} - w_{\text{min}}^{BC} = 1$ (Linsker, 1986a) and applied the equation for the fixed point to go from Eq. (52) to Eq. (53). Note that, since the numerator of Eq. (52) must be negative for the mean weight to be stable (see Eq. (47)), the denominator must also be negative for the size of the on-center to be a real number.

Fig. 4 shows on-center sizes calculated using Eq. (53). From the figure, it can be seen that there is a large range in on-center size, from 1 to 70, and there are large regions of invalid parameter configurations that lead to unstable or complex on-center

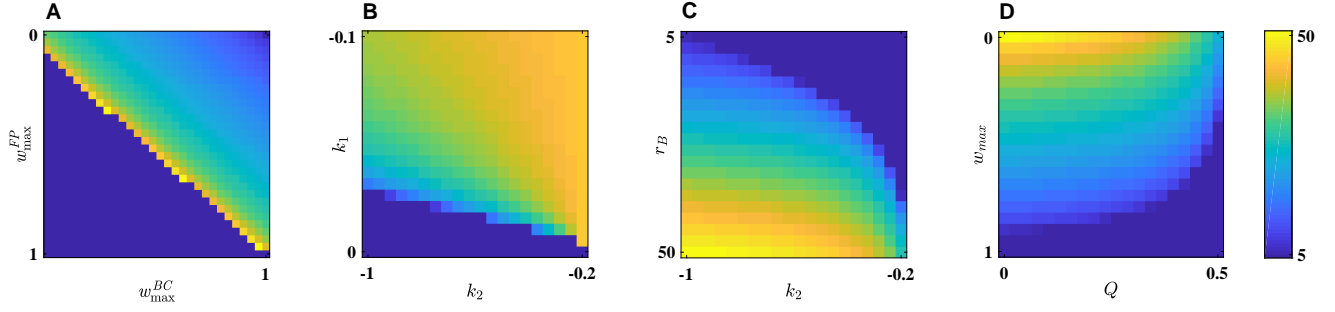


Figure 4: On-center size of layer C cells from Linsker's network, calculated using Eqs. (52) and (53). Propagation delay was assumed equal between all pre- and post-synaptic neurons. Dark blue regions indicate an unstable or complex fixed point, and have consequently been omitted. (C) On-center size as a function of the connectivity radius between layers B and C , and k_2^{BC} , calculated using Eq. (52). Other values were $w_{\max}^{BC} = 0.5$ and $\overline{Q^{BB}} = 0.15 \text{ s}^{-1}$. (D) On-center size as a function of the proportion of excitatory neurons, determined by the upper weight bound Eq. (47), w_{\max}^{BC} , and the average covariance between layer B neurons, calculated using Eq. (52). Other values were $\sigma^{BC} = 30\mu$, where recall that μ denotes the size of the spacing between neurons, $k_1^{BC} = -0.05 \text{ s}^{-1}$ and $k_2^{BC} = -0.6 \text{ s}^{-1}$.

size. For the size to be real and the fixed point (Eq. (48)) to be within the bounds, such that $\overline{w}_*^{BC} \in (w_{\min}^{BC}, w_{\max}^{BC})$, requires $k_2^{BC} + \overline{Q^{BB}} < 0$, $|k_1^{BC}| < |k_2^{BC} + \overline{Q^{BB}}|$ and $\overline{w}_*^{BC} < w_{\max}^{BC}$.

From Eq. (53), it can be seen that to maximize the on-center requires the fixed point weight to approach the maximum synapse weight in value. This is shown in Fig. 4A. The maximum synapse weight is determined by the proportion of excitatory to inhibitory synapses (Linsker, 1986a). For comparatively small mean covariance values, the fixed point weight can be determined by the homeostatic equilibrium parameters, k_1^{BC} and k_2^{BC} , where $k_1^{BC} < k_2^{BC}$ for the mean weight update equation, Eq. (47) to be stable. The ratio of k_1^{BC} to k_2^{BC} must equal the ratio of excitatory synapses to inhibitory synapses in order for the fixed point weight to approach the upper weight bound, and maximize the size of the on-center.

The size of the fixed point mean weight, and hence the size of the on-center, determines how much excitatory versus inhibitory input is received by the cell. To minimize excitation requires minimizing the on-center. From Eq. (53), this can be achieved by maximizing the difference between the fixed point weight and the upper weight bound, which requires minimizing the fixed point weight. From Eq. (48), it can be seen that the fixed point weight is minimized by minimizing k_1^{BC} with respect to $k_2^{BC} + \overline{Q^{BB}}$. That is, spontaneous weight changes should be minimized, as shown in Fig. 4. Additionally, increasing covariance between layer B neurons reduces the fixed point weight, thus improving spatial resolution, which is demonstrated in Fig. 4D.

The relationship between the synaptic connectivity radius, σ^{BC} , and on-center size is shown in Fig. 4C. As connectivity radius increases, mean covariance, $\overline{Q^{BB}}$, decreases. Consequently, the mean synaptic weight is decreased, causing the on-center, Eq. (52), to increase. Additionally, on-center size is scaled by the connectivity radius.

Fig. 4 shows that, with respect to the initial input connectivity radius between layers B and C , σ^{BC} , the final on-center size can be substantially larger or smaller. This is because the radius denotes Gaussian standard deviation, so connections can be made considerably further away from the neuron than the magnitude of the radius. This is important as it demonstrates the versatility of the network in adjusting on-center size according to homeostatic equilibrium parameters and neuron covariance.

3.4.2 Network incorporating a general post-synaptic response

To calculate receptive field size for a network with an arbitrary PSP and identical propagation delays between all neurons, Eq. (52) can be trivially extended to the case for which an arbitrary PSP is incorporated into the neuron model since the impact of the PSP on covariance is to scale it by a constant factor, Eq. (33). Consequently, the expected size of a layer C neuron's receptive field becomes

$$r_{\text{on}}^{\epsilon} = \sigma^{BC} \sqrt{\log \left(\frac{k_2^{BC} + \kappa^{\epsilon} \overline{Q^{BB}}}{w_{\max}^{BC} (k_2^{BC} + \kappa^{\epsilon} \overline{Q^{BB}}) + k_1^{BC}} \right)}. \quad (54)$$

3.4.3 Network incorporating propagation delay and a general post-synaptic response

We now determine expressions for the receptive field size for an arbitrary PSP function and propagation delay that is proportional to the three-dimensional distance between neurons. Using these expressions, a cell's receptive field size will be calculated in this more realistic context.

Introduce the term, $\delta_{\Delta,\varepsilon}^{BC} = vd^{BC}\tau_\varepsilon$, which captures the elements that minimize the spread in arrival time of input spikes to the layer C post-synaptic neuron. As inter-layer distance, d^{BC} , and velocity, v , increase, the impact of radial propagation delay decreases because there is reduced spread in arrival time of spikes that were initiated simultaneously in layer B . As the PSP time constant, τ_ε , increases, the impact of radial propagation delay is reduced because the input signals are low-pass filtered.

Using the expressions for covariance derived in Section 3.3.1, the average covariance into a layer C cell when propagation delay and PSP are incorporated are found to be (see Section F.2 for details)

$$\overline{Q_{\Delta,\varepsilon}^{BB}} = \kappa_{\Delta}^{AB} \frac{4 \left(2 + \frac{(\sigma^{BC})^2}{(\sigma^{AB})^2} \right)}{\left(\frac{(\sigma^{BC})^2}{\delta_{\Delta,\varepsilon}^{BC}} - 2 \right) \left(\frac{(\sigma^{BC})^2}{\delta_{\Delta,\varepsilon}^{BC}} - 2 - 2 \frac{(\sigma^{BC})^2}{(\sigma^{AB})^2} \right) \left(\frac{(\sigma^{BC})^2}{\delta_{\Delta,\varepsilon}^{BC}} + 2 + \frac{(\sigma^{BC})^2}{(\sigma^{AB})^2} \right)}. \quad (55)$$

The impact of delay from propagation between layers is to attenuate covariance, so that $\overline{Q_{\Delta,\varepsilon}^{BB}} \leq \overline{Q^{BB}}$. Attenuation resulting from delay between layers A and B is captured in κ_{Δ}^{AB} , which is itself a function of radial propagation delay, τ_r , and inter-laminar propagation delay, τ_l . For delay between layers B and C , this is captured by the relationship between σ^{BC} and $\delta_{\Delta,\varepsilon}^{BC}$; the larger the connectivity radius, the larger the denominator and the more covariance is attenuated. The radial propagation delay spreads out the arrival time in every consecutive layer pair, compounding the impact of radial delay.

Importantly, for large values of $\delta_{\Delta,\varepsilon}^{BC}$, mean covariance in the presence of propagation delay approaches mean covariance in Linsker's (1986a) network, Eq. (49), since the impact of radial propagation delay becomes negligible, such that

$$\overline{Q_{\Delta,\varepsilon}^{BB}} \xrightarrow{\delta_{\Delta,\varepsilon}^{BC} \rightarrow \infty} \frac{1}{1 + \frac{(\sigma^{BC})^2}{(\sigma^{AB})^2}}. \quad (56)$$

The mean synapse weight converges in the early stages of learning, having a much faster time constant than that of the individual synapses (Kempster et al., 1999b). The learning equation for the mean weight synapse in the presence of propagation delay can be expressed as

$$\dot{\overline{w}}^{BC} = \eta \left(k_1^{BC} + \overline{w}^{BC} \left(k_2^{BC} + \overline{Q_{\Delta,\varepsilon}^{BB}} \right) \right), \quad w_{\min}^{BC} \leq \overline{w}^{BC} \leq w_{\max}^{BC}, \quad (57)$$

so that

$$\overline{w}_*^{BC} = \frac{-k_1^{BC}}{k_2^{BC} + \overline{Q_{\Delta,\varepsilon}^{BB}}}. \quad (58)$$

Consequently, the fixed point of the mean weight is modified by the impact of propagation delay. Since the denominator is negative and $k_2^{BC} < 0$, reducing the size of the mean covariance decreases the size of the mean weight to which the network converges.

Fig. 5 shows a comparison of the fixed point mean synapse weight for Linsker's network, Eq. (49), and the network incorporating propagation delay and arbitrary ε , Eq. (58). Large changes in the homeostatic constant, k_2^{BC} , result in relatively small changes in the fixed point mean weight for the network with propagation delay. In contrast, the same change in homeostatic constant causes the mean weight in Linsker's (1986a) network to change from a value near the lower weight bound to a value to the upper weight bound.

The expected receptive field size after incorporating propagation both delay and an arbitrary PSP function is

$$r_{\text{on}}^{\Delta,\varepsilon} = \sigma^{BC} \sqrt{\log \left(\frac{k_2^{BC} + \overline{Q_{\Delta,\varepsilon}^{BB}}}{w_{\max}^{BC} \left(k_2^{BC} + \overline{Q_{\Delta,\varepsilon}^{BB}} \right) + k_1^{BC}} \right)} \quad (59)$$

$$= \sigma^{BC} \sqrt{\log \left(\frac{1}{w_{\max}^{BC} - \overline{w}_*^{BC}} \right)}, \quad (60)$$

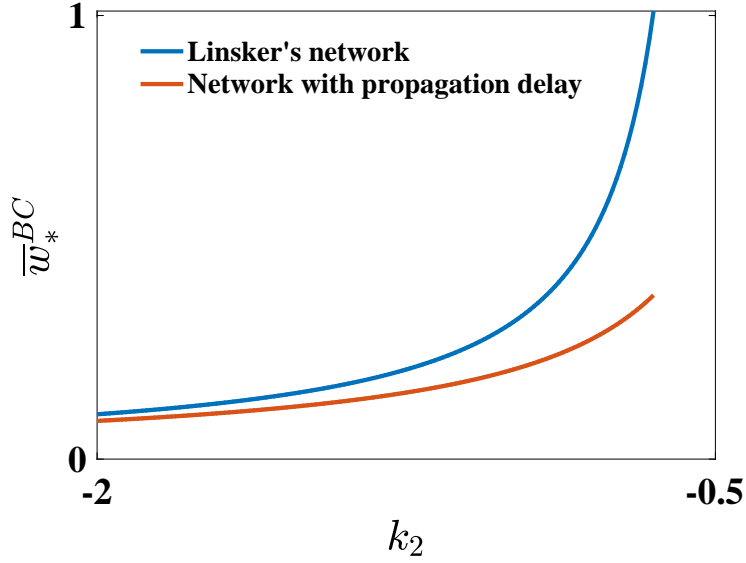


Figure 5: Fixed point mean weight for Linsker's network (Eq. (48), blue line) compared to the fixed point mean weight for the network incorporating propagation delay and an arbitrary PSP (Eq. (58), red line). The figure was generated with $k_1^{BC} = -0.5 \text{ s}^{-1}$, $\overline{Q}^{BB} = 0.5 \text{ s}^{-1}$, Eq. (49), and $\overline{Q}^{BB}_{\Delta,\varepsilon} = 0.24 \text{ s}^{-1}$, Eq. (55). Mean covariance for the network with delay was set assuming that 0.80 of the covariance was retained when neural signals propagated between layers A and B (i.e., $\kappa_{\Delta}^{BC} \kappa_{\varepsilon} = 0.80$), and 0.63 survived propagation between layers B and C.

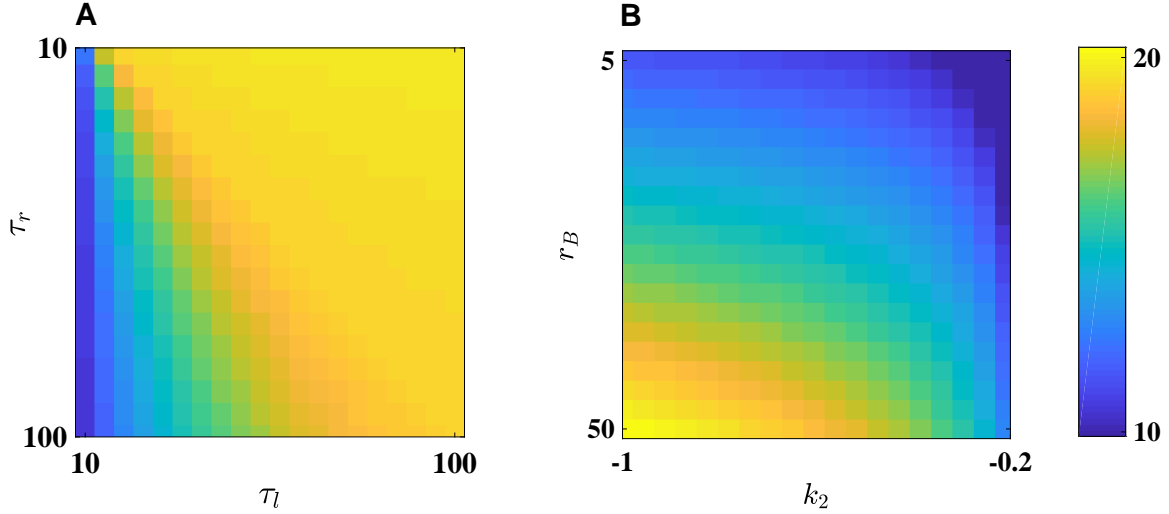


Figure 6: Receptive field size of layer C cells in the network that incorporates propagation delay and an arbitrary PSP, calculated using Eq. (59). **(A)** Receptive field size as a function of covariance between layer B neurons that considers the impact of propagation delay, $\overline{Q}^{BB}_{\Delta,\varepsilon}$. This covariance was adjusted by varying the value of κ_{Δ}^{AB} , in Eq. (55), which depicts the impact of propagation delay between layers A and B. This can be determined by evaluating the impact of inter-layer and radial propagation delays, Eq. (39). Therefore, this figure shows receptive field size as a function of inter-laminar and radial propagation delays between A and B. Other parameter values were $\overline{Q}^{BB} = 0.5 \text{ s}^{-1}$, $\sigma^{BC} = 30 \mu$, $k_1^{BC} = 0.05 \text{ s}^{-1}$ and $k_2^{BC} = -0.5 \text{ s}^{-1}$. **(B)** Receptive field size as a function of σ^{BC} and k_2^{BC} . Other parameter values were $\overline{Q}^{BB} = 0.5 \text{ s}^{-1}$, $k_1^{BC} = 0.05 \text{ s}^{-1}$, $\tau_r = 25 \mu$ and $\tau_l = 100 \mu$.

This equation shows that receptive field size depends on $\overline{Q}^{BB}_{\Delta,\varepsilon}$, which depends on the coefficient, κ_{Δ}^{AB} , Eq. (42), which is itself a function of inter-laminar and radial propagation delays.

Fig. 6 shows receptive field size calculated using Eq. (59). For Fig. 6A, covariance between the layer B neurons that incorporates delay, $\overline{Q}_{\Delta,\varepsilon}^{BB}$, was varied by adjusting the value of κ_{Δ}^{AB} in Eq. (55) to depict the impact of propagation delay between layers A and B . κ_{Δ}^{AB} . The value Eq. (42), was determined from the values of τ_l and τ_r , Eq. (39), using Eq. (40). Fig. 6A illustrates that as the inter-laminar propagation time becomes faster, the impact of radial propagation delay becomes increasingly less significant and, consequently, covariance is less attenuated, the mean synaptic weight increases, and the receptive field size increases. Conversely, as the radial propagation time increases, covariance becomes increasingly attenuated so that there is primarily non-competitive plasticity driving learning. Consequently, the mean synaptic weight becomes smaller and the receptive field size becomes smaller. Therefore, the layer C neurons have comparatively more inhibitory neurons.

Fig. 6 demonstrates that the range in receptive field values is significantly reduced when compared to the range found under the assumption that propagation time is equal between all neurons, shown in Fig. 4. This can be understood by considering Eqs. (58) and (60): receptive field size becomes larger as the fixed point weight approaches the upper bound on the weight. However, the fixed point weight is smaller when propagation delay has been incorporated because the spread in arrival times as the signals traverse between layers attenuates covariance. Consequently, receptive field sizes tend to be smaller.

Fig. 6 also illustrates the smaller range in receptive field values when propagation delay is modelled, when compared to the receptive field sizes exhibited in Fig. 4. This is again because of the larger denominator values caused by the smaller fixed point mean synaptic weights. A similar change in k_2^{BC} values will elicit a smaller change in receptive field size because the denominator is larger in magnitude. Note that when there are proportionally more inhibitory synapses than excitatory synapses, the fixed point weight is negative, Eq. (58), and hence the converse is true: smaller magnitude fixed point weights result in larger receptive field sizes because the denominator of Eq. (60) is comparatively smaller.

3.5 Time constants of convergence of mean synaptic weight

To quantify how propagation delay and PSP functions affect how quickly a cell learns, we evaluate the learning time constant. It has been long established that there are multiple time constants relevant to the evolution of plasticity (Kempster et al., 1999a): the relatively fast evolution of the mean weight, and the much slower evolution of the weights of individual synapses. Initially, we consider the time constant describing the mean weight process, following the method detailed by Kempster et al. (1999a). Given the learning equation for the mean weight in Eq. (47) and the resulting fixed point in Eq. (48), the time constant in converging to the fixed point is given by

$$\overline{\tau}^{BC} = \frac{\overline{w}_*^{BC}}{k_1^{BC}} = -\frac{1}{N^{BC} \left(k_2^{BC} + \overline{Q}^{BC} \right)}. \quad (61)$$

From Section 3.4, it was seen that the fixed point weight for the network incorporating propagation delay and PSP is smaller, Eqs. (48) and (58). Consequently, the time constant for the mean synaptic weight in this network is shorter than for Linsker's (1986a) network.

Conversely, the eigenvalues of the leading eigenfunction of the learning equation incorporating both propagation delay and PSP, Eq. (43), was found to decrease as the impact of delay increased. Propagation delay has a greater impact on the learning equation as the radial propagation time increases with respect to the inter-lamina propagation time through factors such as reduced spike propagation velocity, reduced neural density, and increased synaptic connectivity radii. A decrease in the eigenvalue of the leading eigenfunction implies that learning is slower. Consequently, while the mean synaptic weight is converged upon more quickly, learning of the receptive field structure is a slower process.

3.6 Eigenfunctions of the simplified learning equation with propagation delay

To find the eigenfunctions and eigenvalues for a network model that incorporates propagation delay and an arbitrary postsynaptic potential function, it is necessary to solve the following eigenfunction equation,

$$\lambda w(\mathbf{x}) = A \int_{-\infty}^{\infty} Q \left((f_j^{B(\Delta)} \star \varepsilon)(t - \Delta_{jp}^{BC}), (f_i^{B(\Delta)} \star \varepsilon)(t - \Delta_{ip}^{BC}) \star \varepsilon(t) \right) \exp \left(-\frac{\|\mathbf{x}'\|^2}{(\sigma^{BC})^2} \right) \exp \left(-\frac{\|\mathbf{x}\|^2}{(\sigma^{BC})^2} \right) w(\mathbf{x}') d^2 \mathbf{x}'. \quad (62)$$

To solve Eq. (62), apply the results of Eq. (46) and Eq. (21) with the definition given in Eq. (5). Also note that propagation delay for spikes between the pre-synaptic neuron at \mathbf{x} and the post-synaptic neuron in layer C can be expressed as $\Delta_{\mathbf{x}}^{BC} = \frac{((d^{BC})^2 + \|\mathbf{x}\|^2)^{1/2}}{v}$, which can be approximated by $\Delta_{\mathbf{x}}^{BC} \approx \frac{\|\mathbf{x}\|^2}{2d^{BC}v}$, for inter-laminar distances, d^{BC} , significantly larger than the pre-synaptic neuron's radial distance to the post-synaptic neuron, $\|\mathbf{x}\|$.

$$\lambda w(\mathbf{x}) = A\kappa_{\Delta}^{BC} \int_{-\infty}^{\infty} \exp\left(-\frac{\|\mathbf{x} - \mathbf{x}'\|^2}{2(\sigma^{AB})^2}\right) \exp\left(-\frac{\|\mathbf{x}'\|^2 + \|\mathbf{x}\|^2}{(\sigma^{BC})^2}\right) \exp\left(-\frac{\|\mathbf{x}'\|^2 - \|\mathbf{x}\|^2}{2vd^{BC}\tau_{\epsilon}}\right) w(\mathbf{x}') d^2\mathbf{x}' \quad (63)$$

Converting this to polar coordinates results in

$$\begin{aligned} \lambda w(r, \theta) &= A\kappa_{\Delta}^{BC} \int_0^{\infty} \int_0^{2\pi} \exp\left(-\frac{r^2 + \tilde{r}^2 - 2r\tilde{r}\cos\theta - \tilde{\theta}}{2(\sigma^{AB})^2}\right) \exp\left(-\frac{\tilde{r}^2 + r^2}{(\sigma^{BC})^2}\right) \exp\left(-\frac{|\tilde{r}^2 - r^2|}{2vd^{BC}\tau_{\epsilon}}\right) w(\tilde{r}, \tilde{\theta}) \tilde{r} d\tilde{r} d\tilde{\theta} \\ &= A\kappa_{\Delta}^{BC} \int_0^r \exp\left(-\frac{r^2 + \tilde{r}^2}{2(\sigma^{AB})^2}\right) \exp\left(-\frac{\tilde{r}^2 + r^2}{(\sigma^{BC})^2}\right) \exp\left(-\frac{|\tilde{r}^2 - r^2|}{2vd^{BC}\tau_{\epsilon}}\right) I_0\left(\frac{r\tilde{r}}{(\sigma^{AB})^2}\right) w(\tilde{r}, \tilde{\theta}) \tilde{r} d\tilde{r} d\tilde{\theta} \\ &\quad + A\kappa_{\Delta}^{BC} \int_r^{\infty} \exp\left(-\frac{r^2 + \tilde{r}^2}{2(\sigma^{AB})^2}\right) \exp\left(-\frac{\tilde{r}^2 + r^2}{(\sigma^{BC})^2}\right) \exp\left(-\frac{|\tilde{r}^2 - r^2|}{2vd^{BC}\tau_{\epsilon}}\right) I_0\left(\frac{r\tilde{r}}{(\sigma^{AB})^2}\right) w(\tilde{r}, \tilde{\theta}) \tilde{r} d\tilde{r} d\tilde{\theta}. \end{aligned} \quad (64)$$

This is similar to the learning function for Linsker's (1986a) network, except that it is split into two parts for $\tilde{r} \leq r$ and $\tilde{r} > r$. Given that use of the eigenfunctions for Linsker's (1986a) network in a definite integral that does not cover the entire domain of r leads to an intractable integral, we find the eigenfunctions empirically by following the same procedure as that used for Linsker's network,

$$\begin{aligned} \lambda w(r, \theta) &= A\kappa_{\Delta}^{BC} \int_0^r \exp\left(-\frac{r^2 + \tilde{r}^2}{\beta^2}\right) I_0\left(\frac{r\tilde{r}}{(\sigma^{AB})^2}\right) w(\tilde{r}, \tilde{\theta}) \tilde{r} d\tilde{r} d\tilde{\theta} \\ &\quad + A\kappa_{\Delta}^{BC} \int_r^{\infty} \exp\left(-\frac{r^2 + \tilde{r}^2}{\tilde{\beta}^2}\right) I_0\left(\frac{r\tilde{r}}{(\sigma^{AB})^2}\right) w(\tilde{r}, \tilde{\theta}) \tilde{r} d\tilde{r} d\tilde{\theta}, \end{aligned} \quad (65)$$

where $\beta^2 = \frac{2\delta_{\Delta, \epsilon}^{BC}(\sigma^{BC})^2}{\delta_{\Delta, \epsilon}^{BC}(\sigma^{BC})^2 + 2\delta_{\Delta, \epsilon}^{BC}(\sigma^{AB})^2 + (\sigma^{AB})^2(\sigma^{BC})^2}$, $\tilde{\beta}^2 = \frac{2\delta_{\Delta, \epsilon}^{BC}(\sigma^{BC})^2}{\delta_{\Delta, \epsilon}^{BC}(\sigma^{BC})^2 + 2\delta_{\Delta, \epsilon}^{BC}(\sigma^{AB})^2 - (\sigma^{AB})^2(\sigma^{BC})^2}$, and $\delta_{\Delta, \epsilon}^{BC} = vd^{BC}\tau_{\epsilon}$ captures the elements that spread the arrival time of input spikes to the layer C post-synaptic neuron, as well as the spiking time of the post-synaptic neuron.

Empirically, we determined the eigenfunctions of this learning equation to be

$$\mathbf{v}_{l,n}^{\Delta, \epsilon}(r, \theta) = N_{ln} \kappa_{\Delta}^{BC} \tilde{r}^{l-n} \exp\left(-\frac{r^2}{2C}\right) \left(L_{n+1}^{l-n}\left(\frac{r^2}{C}\right) - L_n^{l-n}\left(\frac{r^2}{C}\right) \right), \quad (66)$$

where $l = 0, 1, \dots, n = 0, 1, \dots, l$, and $C = \frac{\beta}{\sqrt{1-\beta^2}}$.

While the order of the eigenfunctions, as determined by the sizes of their corresponding eigenvalues, changes as a function of velocity, cell density, and interlaminar distance, the leading eigenfunction always remains the same. Fig. 7 shows the eigenfunctions of the learning equation described in Eq. (43). They increasingly differ from those of Linsker's learning equation, Eq. (3.1), as the impact of propagation delay in the radial direction increases, which occurs as a result of decreasing neural density, decreasing propagation velocity, and decreasing interlaminar distance. In response to any of these three factors, the eigenfunctions become increasingly impacted by a sinusoidal function that emanates radially out from the position of the layer C cell. A consequence of this process is that the eigenfunctions are sharpened.

The leading eigenvalue for the simplified learning equation is not a spatial opponent cell, but rather has a receptive field in which center synapses are positive, surrounded by a narrow ring of negative synapses, that tend to zero with increasing distance from the center. As k_2^{BC} decreases, the fixed point mean weight, Eq. (58), becomes smaller, and the ring of inhibitory

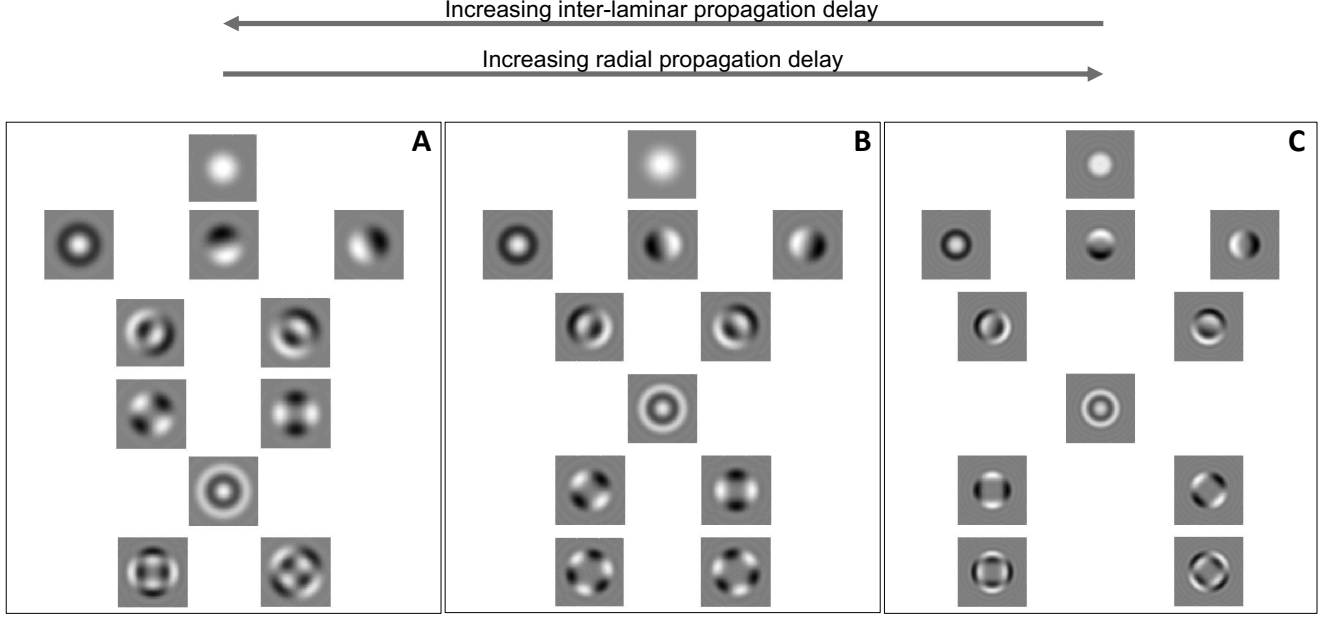


Figure 7: Sets of eigenfunctions for three different networks that incorporate propagation delay. From left to right: radial propagation delay, τ_r , increases, while inter-laminar propagation delay τ_l , becomes relatively shorter. Within each network the eigenvalue decreases as rows are traversed downwards. Eigenfunctions in the same row have the same eigenvalue. The receptive field of a layer C cell is determined by the leading eigenfunction, shown in the top row for each network. Radial and inter-laminar propagation times are as follows: (A) $\tau_r = 25\mu\text{s}$, $\tau_l = 100\mu\text{s}$ (B) $\tau_r = 50\mu\text{s}$, $\tau_l = 50\mu\text{s}$, (C) $\tau_r = 100\mu\text{s}$, $\tau_l = 25\mu\text{s}$. Other parameter values include the synaptic connectivity radius between layers A and B, $\sigma^{AB} = 30\mu$, synaptic connectivity radius between layers B and C, $\sigma^{BC} = 50\mu$, and the time constant for an exponential PSP, $\tau_e = 100\mu\text{s}$.

synapses becomes larger. Consequently, the leading eigenvalue can be seen to become more like a spatial opponent cell, having a positive center and surrounded by synapses with negative weight. While the surrounding negative weights in the eigenfunction may be only very slightly negative, these weights will grow over time until the weight threshold is reached since the structure is unstable.

3.7 Eigenfunctions of the full learning equation

We empirically determined the eigenfunctions of the full learning equation detailed in Eq. (15b). By relaxing the assumption that $k_2 = 0$, the learning equation becomes

$$\lambda w(r, \theta) = A \int \int \left(\kappa_{\Delta}^{BC} \exp\left(-\frac{r^2 + \tilde{r}^2 - 2r\tilde{r}\cos(\theta - \tilde{\theta})}{2(\sigma^{AB})^2}\right) \exp\left(-\frac{|r^2 - \tilde{r}^2|}{2d^{BC\nu}}\right) + k_2^{BC} \right) w(\tilde{r}, \tilde{\theta}) \exp\left(-\frac{\tilde{r}^2 + r^2}{(\sigma^{BC})^2}\right) \tilde{r}d\tilde{r}d\tilde{\theta}, \quad (67)$$

where we have used d instead of d^{BC} to aid readability.

To find the eigenfunctions and eigenvalues of this learning equation, a perturbation analysis must be done as for Linsker's network in Section 3.2. As was the case for Linsker's network, for the perturbation operator defined in Eq. (27), the eigenfunctions for the network with delay are mutually orthogonal. Consequently, the shape of the eigenfunctions remains the same for any. It is therefore only necessary to find the change in each eigenvalue, using $W_{l,n}^{\Delta,\varepsilon} = \langle \mathbf{v}_{l,n}^{\Delta,\varepsilon}(r, \theta) | H^1(r) \theta | \mathbf{v}_{m,p}^{\Delta,\varepsilon}(r, \theta) \rangle$. Empirically, we find that the leading eigenfunction is always the same as the $k_2 = 0$ case, because the eigenvalue perturbation for this eigenfunction is the least negative. Consequently, when added to the eigenvalues of the original system, the leading eigenfunction, which has a positive eigenvalue, continues to have the largest eigenvalue. A cross section of the leading eigenvalue of the learning equation for different values of k_2^{BC} is shown in Fig. 8.

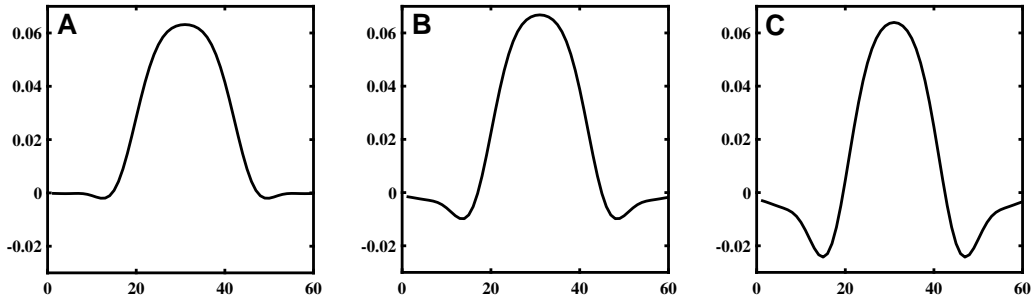


Figure 8: Eigenfunctions of the learning equation when k_2 is included in the learning Eq. (43). (A) $k_2^{BC} = 0$, (B) $k_2^{BC} = -0.5$, (C) $k_2^{BC} = -1$.

4 Discussion

Linsker (1986a) proposed a simple rate-based, three-layered, feed-forward network to show how spatial opponent cells emerge after a period of learning based purely on spontaneous activity and in the absence of external environmental input. Linsker (1986a) demonstrated that Gaussian distributed synaptic connectivity between the layers was sufficient to introduce spatially-dependent correlation in neural outputs, which in turn prompted a self-organizing network. MacKay and Miller (1990) provided a mathematical framework from which to study Linsker’s (1986a) network, while Wimbauer et al. (1998) extended the analysis to include lateral connectivity in the third layer. While these works were formative in establishing a mechanism behind synaptic learning of simple cells prior to birth, they assumed that propagation delay between all neurons was identical and, consequently, had negligible impact.

In this paper, we relaxed the assumption of identical propagation delays in Linsker’s (1986a) network, introducing delay that accounts for both radial distance, i.e. separation within the laminar, and inter-laminar distance, i.e. separation between the layers. We introduced a general post-synaptic potential (PSP) with a finite time course that was interpreted as spreading the probability of a spike over a finite period. The PSP is important as, in its absence, if two pre-synaptic neurons at different distances from the post-synaptic neuron were instantaneously correlated, propagation delay would eliminate the correlation since the activity from the two neurons would arrive at the post-synaptic neurons at different times. Thus, the PSP is crucial to introduce cross-correlation at non-zero lags between the output of the pre-synaptic neurons.

Linsker (1986a) showed that, under Gaussian synaptic connectivity distributions, correlation between two neurons in the second layer was a Gaussian function of their radial separation distance in the laminar. We show that, where propagation time between the first and second layers has been considered and there is a more biophysically realistic PSP, correlation between the outputs of neurons in the second layer can be expressed as a scaled function of correlation between neurons in Linsker’s (1986a) network. That is, when propagation delay and PSP are accounted for, correlation between two neurons in the second layer remains a Gaussian function of their separation distance in the laminar, but is attenuated by a constant, $\kappa_{\Delta,\varepsilon}^{AB}$, that is determined by the mean propagation delay between the first and second layers and the PSP function.

The frequency domain forms of the attenuation functions are shown in Fig. 3. Figs. 3B and 3C show that the impact of propagation delay is to attenuate high frequency information in the neural activity. This result is intuitive since propagation delay spreads out the arrival time of input to the neurons. When the inputs are summed together as they arrive at the post-synaptic neuron, the spread in arrival time filters out the high frequency components of the signal. Fig. 3A shows that, for the case in which propagation time between layers dominates radial propagation time across the laminar, for example $\tau_r = 50\mu\text{s}$ and $\tau_l = 500\mu\text{s}$, delay can be considered approximately equal for the output of all pre-synaptic neurons and, hence, all frequency components are retained. As the impact of radial propagation delay becomes more severe by increasing the synaptic connectivity radius, reducing neuron density, reducing propagation velocity, or reducing the inter-laminar distance, the spread in signal arrival times from the previous layer becomes more dispersed and an increasing proportion of the high frequencies are attenuated. For example, when $\tau_r = 250\mu\text{s}$ and $\tau_l = 500\mu\text{s}$, the cut-off frequency is approximately half the Nyquist frequency, and when $\tau_r = 500\mu\text{s}$ and $\tau_l = 500\mu\text{s}$, the cut-off frequency is about one quarter of the Nyquist frequency. Consequently, propagation delay acts like a low-pass filter, where the cut-off frequency is determined by the relationship of the radial propagation delay to the inter-laminar propagation delay.

Fig. 3D shows a frequency domain plot of an exponential PSP to allow comparison with the mean delay function. The PSP time constants were chosen to reflect the effective membrane time constant, which is shorter than the membrane time constant due to the neuron becoming more leaky as more synaptic channels open with increased activity (Burkitt et al., 2003). The figure shows plots for effective time constants between 0.1ms and 10ms. It is immediately evident that, for longer effective time constants, the impact of propagation delay is to attenuate high frequencies that are not present in the signal after it has been convolved with the PSP. However, for shorter effective time constants or for neurons that incur a longer radial propagation time, propagation delay can significantly attenuate frequencies that are present in the covaried input to the post-synaptic neuron. Therefore, the effective time constant of each should enable the processing of similar scales of temporal information. This is indeed the situation in the retina, where time constants at the periphery have been found to be up to twice as long as those in the fovea, where neurons are much more densely packed (Sinha et al., 2017).

The change in frequency content of the summed input to a post-synaptic neuron as radial propagation delay becomes more prominent may explain other experimental results in the visual system. In the visual system, it has been found that contrast sensitivity is frequency dependent in the periphery, such that sensitivity decreases for higher frequencies (Venkataraman et al., 2017). This agrees with our results since neurons that are more spread out receive input that is attenuated at higher frequencies and thus higher amplitude input is required to obtain a similar response. Additionally, Thibos et al. (1996) demonstrated that cut-off frequency is a function of eccentricity such that it decreases as distance from the fovea increases. This accords with our results; as the impact of radial delay increases with distance from the fovea, delay acts like a low-pass filter, where the cut-off frequency decreases as neurons become more spread across the laminar.

Linsker (1986a) empirically demonstrated that spatial-opponent cells develop in the third layer of his proposed network, emerging as a consequence of the Gaussian synaptic connectivity. MacKay and Miller (1990) studied the dynamics of Linsker’s (1986a) network and provided the first six eigenfunctions of the learning equation with homeostatic parameters set to zero, by proposing the solution forms and substituting them into the learning equation to prove that they behaved as eigenfunctions. We analytically derived the full set of eigenfunctions and eigenvalues for Linsker’s (1986a) network and extended these results to non-zero homeostatic parameters, showing that the leading eigenfunction for Linsker’s (1986a) network can change (Davey et al., 2018). Consequently, the resulting cell structure in the third layer, which is determined by the leading eigenfunction, can change from a spatial-opponent cell to a bi-lobed cell, which was also noted by MacKay and Miller (1990). A cut-off value for the homeostatic constants that triggers the change in eigenfunction can be determined from our analytical results.

In this paper, we empirically determined the eigenfunctions for the network incorporating propagation delay and PSP. We showed that, for this network, the leading eigenfunction is stable for all values of the homeostatic parameters. This result appears sensible as it avoids a potentially infinitesimally small change in homeostatic parameters triggering a change in cell structure. Furthermore, the leading eigenfunction has a much sharper boundary between the ON and OFF regions when the impact of delay is considered (Fig. 7).

The final contribution of this paper was to consider the size of the on-center of the spatial opponent cell that emerge in the third layer. This was determined by calculating the fixed point for the mean synaptic weight and establishing how large the on component was required to be to establish the fixed point mean weight. The learning equation for the mean weight is stable only when the competitive plasticity, Q , component is negative and larger in magnitude than the non-competitive component, k_2 . The competitive component is comprised of a negative constant and the positive mean covariance between the pre-synaptic inputs. If the mean covariance approaches the constant in magnitude, the fixed point weight becomes increasingly large until it reaches a point of instability. Furthermore, as the fixed point weight approaches the upper weight bound, the size of the cell’s on-center increases rapidly.

When propagation delay is incorporated into the network, the fixed point weight, and hence the on-center size of the spatial opponent cell, is much more stable to changes in homeostatic parameters and factors that determine covariance. Fig. 5 shows the fixed point mean synaptic weight for both Linsker’s (1986a) network and the network with propagation delay. A small change in homeostatic constant can trigger a large change in the fixed point weight in Linsker’s (1986a) network, and hence a large change in the receptive field structure of the cell. The fixed point weight for the network with propagation delay is comparatively stable. The region of instability for Linsker’s (1986a) is largely avoided since covariance is attenuated and hence the fixed point weight never approaches the upper bound.

We show that a small connectivity radius, in addition to densely packed cells and consequently negligible radial propagation delay, both act to maintain large covariances between pre-synaptic inputs. The consequence of this is a larger mean synaptic weight and comparatively larger on-center. Therefore, densely packed cells with small connectivity radii have mostly excitatory input, and very little inhibitory input. Conversely, cells that are more spread out and more likely to connect to neurons

further away have a smaller mean synaptic weight, which results in a smaller on-center. Therefore, these cells have more inhibitory input. This is indeed what is found in the retina, where cells in the fovea have very little inhibitory input, whereas cells in the periphery have significantly more inhibitory input, with a more than 10-fold change between foveal and peripheral cells (Sinha et al., 2017).

Acknowledgements

The authors acknowledge support under the Australian Research Council’s Discovery Projects funding scheme (Project DP140102947).

CED acknowledges support under the University of Melbourne Research Fellowship.

Appendix A Expected number of shared inputs

To examine network dynamics, it is necessary to ascertain the expected number of shared connections between two neurons. The number of shared connections from a presynaptic layer to two neurons in the postsynaptic layer, say i and j , depends on the radial distance between them since the synaptic connection density for each is a Gaussian function of distance (see Fig. 1). We assume for simplicity and without loss of generality that i and j differ only in their x coordinate so that $d_{ij}^B = x_{mi} - x_{mj}$.

Center the Cartesian coordinates describing a neuron’s position in the laminar on one of the postsynaptic neurons, say i , so that the other postsynaptic neuron, say j , lies on the x axis. From Eq. (1), neuron m , in layer A , has a probability of connecting to neuron i in layer B of $p_N(x_{mi}, y_{mi}; \mathbf{0}, \Sigma^A)$ and a probability of connecting to neuron j in layer B of $p_N(x_{mj}, y_{mj}; \mathbf{0}, \Sigma^A) = p_N(x_{mi} - d_{ij}^B, y_{mi}; \mathbf{0}, \Sigma^A)$. The probability of the presynaptic neuron connecting to both postsynaptic neurons i and j is simply the product of the probability of each individual connection being made. The expected number of common connections can be determined by summing this joint probability over the layer or, in the continuous limit, integrating the joint probability over the layer of presynaptic neurons. If N^{AB} denotes the number of synaptic connections from layer A to a layer B neuron and $N^{BB}(d)$ the number of shared connections between two postsynaptic neurons in layer B separated by a distance of d , then in the continuous limit,

$$N^{BB}(d) = (N^{AB})^2 \iint_{xy} p_N(x, y; \mathbf{0}, \Sigma^A) p_N(x - d, y; \mathbf{0}, \Sigma^A) dx dy, \quad (68)$$

where the sub- and super-scripts on distance parameters have been dropped to aid readability. This can be expanded as

$$\begin{aligned} N^{BB}(d) &= (N^{AB})^2 \iint_{xy} \frac{1}{(\pi(\sigma^{AB})^2)^2} \exp\left(-\frac{x^2 + y^2}{(\sigma^{AB})^2}\right) \exp\left(-\frac{(x-d)^2 + y^2}{(\sigma^{AB})^2}\right) dx dy \\ &= \frac{(N^{AB})^2}{(\pi(\sigma^{AB})^2)^2} \iint_{xy} \exp\left(-\frac{2x^2 + 2y^2 + d^2 - 2xd}{(\sigma^{AB})^2}\right) dx dy \\ &= \frac{(N^{AB})^2}{(\pi(\sigma^{AB})^2)^2} \iint_{xy} \exp\left(-\frac{2\left(\left(x - \frac{d}{2}\right)^2 + y^2 + \frac{d^2}{4}\right)}{(\sigma^{AB})^2}\right) dx dy. \end{aligned} \quad (69)$$

Introduce $x' = x - d/2$, so that

$$\begin{aligned}
N^{BB}(d) &= \exp\left(-\frac{d^2}{2(\sigma^{AB})^2}\right) \frac{(N^{AB})^2}{(\pi(\sigma^{AB})^2)^2} \iint_{xy} \exp\left(-\frac{2(x'^2 + y^2)}{(\sigma^{AB})^2}\right) dx dy \\
&= \exp\left(-\frac{d^2}{2(\sigma^{AB})^2}\right) \frac{(N^{AB})^2}{(\pi(\sigma^{AB})^2)^2} \sqrt{\frac{\pi(\sigma^{AB})^2}{2}} \sqrt{\frac{\pi(\sigma^{AB})^2}{2}} \\
&= \frac{(N^{AB})^2}{2\pi(\sigma^{AB})^2} \exp\left(-\frac{d^2}{2(\sigma^{AB})^2}\right), \tag{70}
\end{aligned}$$

using the identity $\int_{-\infty}^{\infty} \exp(-ax^2) = \sqrt{\pi/a}$.

This result demonstrates that the number of shared connections between two neurons with Gaussian synaptic connection densities is itself a Gaussian function of the radial distance between the neurons with a variance that is half the value of the synaptic connection density radius. This means that a postsynaptic neuron is expected to have the most common connections with itself, for which $d = 0$. Additionally, for small variance or connection radius, a postsynaptic neuron will share many connections with proximate neighbors, with the number of shared connections falling off quickly with distance. Since the expected number of synaptic inputs is constant, a large connection radius implies that the neuron will have shared connections with neurons comparatively distal to it, since nearby neurons will have comparatively fewer shared connections.

Appendix B Variance of neural activity

To derive the variance in neural activity for a layer B neuron, it is necessary to consider that a single presynaptic neuron, say neuron m , in layer A may have multiple synaptic connections to a neuron i in layer B (see Fig. 1). Using the synaptic connection density in Eq. (1), we know that the expected number of synaptic connections between m and i , separated by a distance of $[x_{mi}, y_{mi}]$, is

$$N_{mi}^{AB} = \frac{N^{AB}}{\pi(\sigma^{AB})^2} \exp\left(-\frac{x_{mi}^2 + y_{mi}^2}{(\sigma^{AB})^2}\right). \tag{71}$$

From Eq. (6a), the expected variance of a neuron in layer B can be written as,

$$\begin{aligned}
\text{var}(\langle f_i^B \rangle) &= \text{var}\left(\left\langle R_a^B + \sum_m w_{mi}^{BC} f_m^A \right\rangle\right) \\
&= N^{AB} \lambda^A + 2 \sum_m \sum_{n < m} \langle \text{cov}(f_m^A, f_n^A) \rangle, \tag{72}
\end{aligned}$$

where we have assumed that weights between layers A and B have evolved to the upper bound of 1 (cf. Linsker (1986a)) and used the fact that $\text{var}\left(\sum_{i=1}^n a_i x_i\right) = \sum_{i=1}^n a_i^2 \text{var}(x_i) + 2 \sum_j \sum_{i < j} a_i a_j \text{cov}(x_i, x_j)$.

To determine the contribution of the covariance term in Eq. (72), we note that each pair of synapses originating from the same presynaptic neuron will be fully correlated, while synapses stemming from different presynaptic neurons in layer A will be uncorrelated. For neuron m in layer A with N_{mi}^{AB} synaptic connections to neuron i in layer B , there will be $\binom{N_{mi}^{AB}}{2} = N_{mi}^{AB} (N_{mi}^{AB} - 1) / 2 \approx (N_{mi}^{AB})^2 / 2$ synapse pairs contributing to the covariance sum. Consequently, the total contribution of neuron m to the covariance term in Eq. (72) will be $\frac{(N_{mi}^{AB})^2}{2} \lambda^A$. To obtain an expression for the variance of layer B neurons, we evaluate this expression using Eq. (71) and substitute it into Eq. (72). Applying a continuous spatial approximation to the layer, we can integrate to get the total expected contribution of all presynaptic neurons to the covariance term and evaluate

Eq. (72),

$$\begin{aligned}
\text{var}(\langle f_i^B \rangle) &= N^{AB} \lambda^A + \lambda^A \iint_{xy} N_{mi}^2 dx dy \\
&= N^{AB} \lambda^A + \lambda^A \iint_{xy} \left(\frac{N^{AB}}{\pi(\sigma^{AB})^2} \right)^2 \exp\left(-2 \frac{x^2 + y^2}{(\sigma^{AB})^2}\right) dx dy \\
&= \lambda^A \left(N^{AB} + \frac{(N^{AB})^2}{2\pi(\sigma^{AB})^2} \right). \tag{73}
\end{aligned}$$

Appendix C Covariance of neural activity

We wish to derive expressions for the covariance of layer B neurons. Sample covariance between two postsynaptic neuron rates in layer B , say f_i^B and f_j^B , for neurons i and j , respectively, is calculated as

$$\text{cov}(f_i^B, f_j^B) = \mathbb{E}[f_i^B f_j^B] - \mathbb{E}[f_i^B] \mathbb{E}[f_j^B]. \tag{74}$$

For unitary weights from layer A to layer B , Eq. (6) can be employed to give

$$\begin{aligned}
\text{cov}(f_i^B, f_j^B) &= \mathbb{E}\left[\left(R_a^B + \sum_m f_m^A\right)\left(R_a^B + \sum_n f_n^A\right)\right] - \mathbb{E}\left[R_a^B + \sum_m f_m^A\right] \mathbb{E}\left[R_a^B + \sum_n f_n^A\right] \\
&= (R_a^B)^2 + 2R_a^B \overline{f^B} + \mathbb{E}\left[\sum_m \sum_n f_m^A f_n^A\right] - \left((R_a^B)^2 + 2R_a^B \overline{f^B} + (N^{AB} \overline{f^B})^2\right) \\
&= \left(\mathbb{E}\left[\sum_m \sum_n f_m^A f_n^A\right] - (N^{AB} \overline{f^B})^2\right). \tag{75}
\end{aligned}$$

Layer A neurons are uncorrelated so that the only non-zero contribution to this sum occurs when a layer A neuron has a synaptic connection to each of the layer B neurons under consideration. In this case, the input rates are fully correlated so that the contribution to covariance is proportional to the layer A firing rate squared, $(\lambda^A)^2$.

Using the expression for the expected number of shared connections between layer B neurons in Eq. (3), the covariance is given by

$$\text{cov}(f_i^B, f_j^B) = \frac{(N^{AB})^2 (\lambda^A)^2}{2\pi(\sigma^{AB})^2} \exp\left(-\frac{d^2}{2(\sigma^{AB})^2}\right). \tag{76}$$

Appendix D Covariance of neural activity in the frequency domain

We express covariance between two stationary, real variates, x and y , as a function of their frequency domain counterparts, X and Y .

$$\gamma_{x,y}(\tau) = \frac{1}{T} \sum_t X(t) Y(t + \tau). \tag{77}$$

Similar to the convolution theorem, the cross-correlation theorem states that (Kumar, 2009)

$$\gamma_{x,y}(\tau) = \frac{1}{T^2} \sum_k (X(k))^* Y(k) \exp\left(2\pi i \tau \frac{k}{T}\right), \tag{78}$$

where $X(k)$ and $Y(k)$ denote the spectral variates of x and y , respectively, at frequency k .

Since instantaneous covariance is equivalent to the cross-correlation of zero-meanded variates at lag 0, we can express covariance between two layer B neurons as

$$\begin{aligned}\text{cov}(f_i^B, f_j^B) &= \frac{1}{T^2} \sum_k (F_i^B(k))^* F_j^B(k) \exp\left(2\pi i 0 \frac{k}{T}\right) \\ &= \frac{1}{T^2} \sum_k (F_i^B(k))^* F_j^B(k).\end{aligned}\quad (79)$$

Appendix E Derivation of delay in the frequency domain

We wish to calculate the expected value of delay in the frequency domain. This requires an expression of delay as a function of distance in the frequency domain and the probability of obtaining each distance. The product of these two functions can then be integrated over the laminar to give the expected value. Since we are finding the expected value in the frequency domain, we can expect values to be complex. Consequently, contour integration will be used.

To calculate the expected value of delay in the frequency domain, use $E[d] = \int g(d)p(d)dr$ for some function, $g(d)$, of distance, d , with probability density, $p(d)$. Using the known distribution of distance, given in Eq. (4), the linear transformation from distance to delay, given in Eq. (5), and the expression of a temporal delay in the frequency domain, given by $\mathcal{F}\{x(t - \Delta)\} = X(k) \exp(-2\pi i \Delta k')$, the function can be identified as $g(d) = \exp\left(-2\pi i k'/T \frac{((d^{AB})^2 + d^2)^{1/2} \mu}{v}\right)$. Consequently, the expected value of delay in the frequency domain can be determined by evaluating

$$E[\exp(-2\pi i \Delta k')] = \int_0^\infty \exp\left(-2\pi i k' \frac{((d^{AB})^2 + d^2)^{1/2} \mu}{v}\right) \frac{2d}{(\sigma^{AB})^2} \exp\left(-\frac{d^2}{(\sigma^{AB})^2}\right) dd, \quad (80)$$

where we have used $d_{mi}^B = d$. Introduce a change of variable, $r' = ((d^{AB})^2 + d^2)^{1/2}$, so that $dd = dr' (r'^2 - (d^{AB})^2)^{-1/2} r'$, and

$$\begin{aligned}E[\exp(-2\pi i \Delta k')] &= \frac{2}{(\sigma^{AB})^2} \int_{d^{AB}}^\infty r' \exp\left(-2\pi i k' \frac{r' \mu}{v}\right) \exp\left(-\frac{r'^2 - (d^{AB})^2}{(\sigma^{AB})^2}\right) dr' \\ &= \frac{2}{(\sigma^{AB})^2} \exp\left(\frac{(d^{AB})^2}{(\sigma^{AB})^2}\right) \int_{d^{AB}}^\infty r' \exp\left(-\frac{r'^2}{(\sigma^{AB})^2}\right) \exp\left(-2\pi i k' \frac{r' \mu}{v}\right) dr'.\end{aligned}\quad (81)$$

This integral has the form $\int_{x_0}^\infty x e^{-ax^2} e^{-ibx} dx$, which we will use for the interim for readability. Using integration by parts,

$$\int_{x_0}^\infty f(x)g'(x)dx = f(x)g(x) \Big|_{x_0}^\infty - \int_{x_0}^\infty g(x)f'(x)dx, \quad (83)$$

and setting $g(x) = -\frac{1}{2a}e^{-ax^2}$, $f(x) = e^{-ibx}$, so that $g'(x) = xe^{-ax^2}$, and $f'(x) = -ibe^{-ibx}$, and

$$\begin{aligned}\int_{x_0}^\infty x e^{-ax^2} e^{-ibx} dx &= -\frac{1}{2a} e^{-ibx} e^{-ax^2} \Big|_{x_0}^\infty - \frac{1}{2a} \int_0^\infty ibe^{-ibx} e^{-ax^2} dx \\ &= +\frac{1}{2a} e^{-ax_0^2 - ibx_0} + \frac{ib}{2a} - \int_{x_0}^\infty e^{-(ax^2 + ibx)} dx.\end{aligned}\quad (84)$$

Since the integral in Eq. (84) is over a complex domain, it can be solved using contour integration. Cauchy's theorem states that, for an analytic function that is differentiable everywhere, a closed line integral of the function evaluates to zero.

Consequently, in general,

$$0 = \oint e^{-ax^2} dx \quad (85)$$

$$= \int_{x_0}^{\infty} e^{-a(x+iz)^2} dx \Big|_{z=0} + i \int_0^p e^{-a(x+iz)^2} dz \Big|_{x=\infty} - \int_{x_0}^{\infty} e^{-a(x+iz)^2} dx \Big|_{z=p} - i \int_0^p e^{-a(x+iz)^2} dz \Big|_{x=0}, \quad (86)$$

$$(87)$$

where the contour is from $x_0 + i0 \rightarrow \infty + i0$, then $\infty + i0 \rightarrow \infty + ip$, from $\infty + ip \rightarrow x_0 + ip$, and finally $x_0 + ip \rightarrow x_0 + i0$. The second term on the right-hand side evaluates to 0 since it contains $e^{-\infty}$, so that

$$0 = \oint e^{-ax^2} dy \quad (88)$$

$$= \int_{x_0}^{\infty} e^{-ax^2} dy - \int_{x_0}^{\infty} e^{-a(x+ip)^2} dy - i \int_0^p e^{-a(x_0+iz)^2} dz. \quad (89)$$

$$(90)$$

Using the fact that $\int_{-\infty}^{\infty} e^{-ax^2} = \sqrt{\frac{\pi}{a}}$, in conjunction with e^{-ax^2} being a real function, we know that $\int_0^{\infty} e^{-ax^2} = \sqrt{\frac{\pi}{4a}}$. Therefore,

$$\begin{aligned} \int_{x_0}^{\infty} e^{-a(x+ip)^2} dx &= \int_{x_0}^{\infty} e^{-ax^2} dy - i \int_0^p e^{-a(x_0+iz)^2} dz \\ &= \sqrt{\frac{\pi}{4a}} \operatorname{erfc}(\sqrt{ax}) - i \sqrt{\frac{\pi}{4a}} (\operatorname{erf}(\sqrt{ap}(x_0 + ip)) - \operatorname{erf}(\sqrt{ax_0})) \\ &= \sqrt{\frac{\pi}{4a}} (\operatorname{erfc}(\sqrt{ax}) - \operatorname{ierf}(\sqrt{a}(x_0 + ip)) + \operatorname{ierf}(\sqrt{ax_0})) \end{aligned} \quad (91)$$

where we have used the definition of $\operatorname{erfi}(z) = \frac{2}{\sqrt{\pi}} \int_0^z e^{t^2} dt$, followed by $\operatorname{erfi}(z) = -\operatorname{ierf}(iz)$.

For the specific integral of $e^{-(ax^2+ibx)}$, set $p = \frac{b}{2a}$,

$$e^{-a(x+ip)^2} = e^{-a(x+i\frac{b}{2a})^2} \quad (92)$$

$$= e^{-ax^2-ibx} e^{\frac{b^2}{4a}}, \quad (93)$$

so that, from Eq. (91),

$$e^{-(ax^2+ibx)} e^{\frac{b^2}{4a}} = \sqrt{\frac{\pi}{4a}} \left(\operatorname{erfc}(\sqrt{ax}) - \operatorname{ierf}\left(\sqrt{a}\left(x_0 + i\frac{b}{2a}\right)\right) + \operatorname{ierf}(\sqrt{ax_0}) \right), \quad (94)$$

or

$$e^{-ax^2} e^{-ibx} = e^{\frac{-b^2}{4a}} \sqrt{\frac{\pi}{4a}} \left(\operatorname{erfc}(\sqrt{ax}) - \operatorname{ierf}\left(\sqrt{ax_0} + i\frac{b}{2\sqrt{a}}\right) + \operatorname{ierf}(\sqrt{ax_0}) \right). \quad (95)$$

Substituting this result back into Eq. (84), we get

$$\begin{aligned} \int_{x_0}^{\infty} x e^{-ax^2} e^{-ibx} dx &= \frac{1}{2a} - \frac{ib\sqrt{\pi}}{4a^{3/2}} e^{\frac{-b^2}{4a}} \left(\operatorname{erfc}(\sqrt{ax_0}) - \operatorname{ierf}\left(\sqrt{ax_0} + i\frac{b}{2\sqrt{a}}\right) + \operatorname{ierf}(\sqrt{ax_0}) \right) \\ &= \frac{1}{2a} e^{-ax_0^2-ibx_0} - \frac{b\sqrt{\pi}}{4a^{3/2}} e^{\frac{-b^2}{4a}} \left(\operatorname{ierfc}(\sqrt{ax_0}) + \operatorname{erf}\left(\sqrt{ax_0} + i\frac{b}{2\sqrt{a}}\right) - \operatorname{erf}(\sqrt{ax_0}) \right). \end{aligned} \quad (96)$$

Applying this result to the original equation in Eq. (81) using $a = \frac{1}{(\sigma^{AB})^2}$, $b = 2\pi k' \frac{\mu}{v}$, and $x_0 = d^{AB}$, the expected value of delay between layers A and layer B is

$$\begin{aligned}
D^{AB}(k) &= \mathbb{E} \left[\exp(-2\pi i \Delta k') \right] \\
&= \exp \left(-2\pi i k' \frac{d^{AB} \mu}{v} \right) \\
&\quad - \pi^{3/2} k' \frac{\sigma^{AB} \mu}{v} \exp \left(\frac{(d^{AB})^2}{(\sigma^{AB})^2} \right) \exp \left(- \left(\pi k' \frac{\sigma^{AB} \mu}{v} \right)^2 \right) \left(\operatorname{ierfc} \left(\frac{d^{AB}}{\sigma^{AB}} \right) + \operatorname{erf} \left(\frac{d^{AB}}{\sigma^{AB}} + i \pi k' \frac{\sigma^{AB} \mu}{v} \right) - \operatorname{erf} \left(\frac{d^{AB}}{\sigma^{AB}} \right) \right).
\end{aligned} \tag{97}$$

For $d^{AB} \gg \sigma^{AB}$, this reduces to $\mathbb{E} \left[\exp \left(-2\pi i k' \frac{d^{AB} \mu}{v} \right) \right]$ which has an absolute value of 1.

Appendix F Derivation of average covariance

F.1 Linsker's network

The average covariance between layer B neurons in the network assumed by Linsker (1986a) can be found by integrating the expression for covariance over the laminar,

$$\begin{aligned}
\overline{Q^{BB}} &= \frac{1}{(\pi(\sigma^{BC})^2)^2} \int_{-\infty}^{\infty} \int_{-\infty}^{\infty} \exp \left(-\frac{|\mathbf{x} - \mathbf{x}'|^2}{2(\sigma^{AB})^2} \right) \exp \left(-\frac{(\mathbf{x}^2 + \mathbf{x}'^2)}{(\sigma^{BC})^2} \right) d\mathbf{x}' d\mathbf{x} \\
&= \frac{1}{(\pi(\sigma^{BC})^2)^2} \exp \left(-\frac{\mathbf{x}^2}{\alpha} \right) \int_{-\infty}^{\infty} \int_{-\infty}^{\infty} \exp \left(-\frac{\mathbf{x}'^2}{\alpha} \right) \exp \left(\frac{\mathbf{x}' \mathbf{x}}{(\sigma^{AB})^2} \right) d\mathbf{x}' d\mathbf{x}
\end{aligned} \tag{98}$$

where $\alpha = \frac{2(\sigma^{AB})^2(\sigma^{BC})^2}{2(\sigma^{AB})^2 + (\sigma^{BC})^2}$ for convenience. Furthermore, the radial symmetry of the covariance and probability connection functions renders the result directionally invariant. Therefore, we calculate the result in one dimension and square it to

generalize it to two dimensions,

$$\begin{aligned}
\overline{Q^{BB}} &= \frac{1}{(\pi(\sigma^{BC})^2)^2} \left(\int_{-\infty}^{\infty} \exp\left(-\frac{x^2}{\alpha}\right) \exp\left(\frac{x^2 \alpha}{4(\sigma^{AB})^4}\right) \int_{-\infty}^{\infty} \exp\left(-\left(\frac{x}{\alpha} - \frac{\sqrt{\alpha}\tilde{x}}{2(\sigma^{AB})^2}\right)^2\right) d\tilde{x} dx \right)^2 \\
&= \frac{\pi\alpha}{(\pi(\sigma^{BC})^2)^2} \left(\int_{-\infty}^{\infty} \exp\left(-\frac{x^2}{\alpha}\right) \exp\left(\frac{x^2 \alpha}{4(\sigma^{AB})^4}\right) \exp(-\chi^2) d\chi dx \right)^2 \\
&= \frac{\alpha}{\pi(\sigma^{BC})^4} \left(\int_{-\infty}^{\infty} \exp\left(-x^2 \frac{4(\sigma^{AB})^4 - \alpha^2}{4(\sigma^{AB})^2 \alpha}\right) dx \right)^2 \\
&= \frac{\alpha}{\pi(\sigma^{BC})^4} \left(\int_{-\infty}^{\infty} \exp\left(-x^2 \frac{2(\sigma^{AB})^2 + (\sigma^{BC})^2}{2(\sigma^{AB})^2(\sigma^{BC})^2 + (\sigma^{BC})^4}\right) dx \right)^2 \\
&= \frac{\alpha}{\pi(\sigma^{BC})^4} \left(\frac{\pi(2(\sigma^{AB})^2(\sigma^{BC})^2 + (\sigma^{BC})^4)}{2(\sigma^{AB})^2 + 2(\sigma^{BC})^4} \right)^2 \\
&= \frac{2(\sigma^{AB})^4 + (\sigma^{AB})^2(\sigma^{BC})^2}{2(\sigma^{AB})^4 + 3(\sigma^{AB})^2(\sigma^{BC})^2 + (\sigma^{BC})^4} \\
&= \frac{2 + \frac{(\sigma^{BC})^2}{(\sigma^{AB})^2}}{2 + 3\frac{(\sigma^{BC})^2}{(\sigma^{AB})^2} + \frac{(\sigma^{BC})^4}{(\sigma^{AB})^4}} \\
&= \frac{2 + \frac{(\sigma^{BC})^2}{(\sigma^{AB})^2}}{\left(2 + \frac{(\sigma^{BC})^2}{(\sigma^{AB})^2}\right) \left(1 + \frac{(\sigma^{BC})^2}{(\sigma^{AB})^2}\right)} \\
&= \frac{1}{1 + \frac{(\sigma^{BC})^2}{(\sigma^{AB})^2}}. \tag{99}
\end{aligned}$$

F.2 Network with propagation delay and arbitrary post-synaptic potential function

For a network that incorporates the impact of delay and an arbitrary PSP function, the average covariance of the pre-synaptic inputs to the post-synaptic neurons in layer C must be calculated using the expression for covariance between two filtered and delayed layer B neuron outputs, since the signals arrive at the synapse where learning is assumed to occur. This expression was determined in Eq. (45), where it was assumed that synapse weight changes are initiated near the cell body of the post-synaptic neuron. To calculate the average normalized covariance, Eq. (16), we use Cartesian coordinates, recognizing that the expression for covariance is circularly symmetric. Therefore, we determine the result for a single dimension and square it. We first find the average covariance for a neuron at position \mathbf{x} with all other neurons in the laminar, and then find the average across all neurons. Propagation delay for spikes between the pre-synaptic neuron at \mathbf{x} and the post-synaptic neuron in layer C can be expressed as $\Delta_{\mathbf{x}}^{BC} = \frac{((d^{BC})^2 + \|\mathbf{x}\|^2)^{1/2}}{v}$, which can be approximated by $\Delta_{\mathbf{x}}^{BC} \approx \frac{\|\mathbf{x}\|^2}{2d^{BC}v}$ for inter-laminar distances, d^{BC} , significantly larger than the pre-synaptic neuron's radial distance to the post-synaptic neuron, $\|\mathbf{x}\|$. Mean covariance can then

be expressed as

$$\begin{aligned}
\overline{Q_{\Delta,\varepsilon}^{BB}} &\approx \frac{\kappa_{\Delta}^{BC}}{\pi^2(\sigma^{BC})^4} \left(\int_{-\infty}^{\infty} dx \int_{-\infty}^{\infty} d\tilde{x} \exp\left(-\frac{x^2 + \tilde{x}^2}{2(\sigma^{AB})^2}\right) \exp\left(\frac{x\tilde{x}}{(\sigma^{AB})^2}\right) \exp\left(-\frac{x^2 + \tilde{x}^2}{(\sigma^{BC})^2}\right) \exp\left(-\frac{|x^2 - \tilde{x}^2|}{2d^{BC}v}\right) \right)^2 \\
&= \frac{\kappa_{\Delta}^{BC}}{\pi^2(\sigma^{BC})^4} \left(\int_{-\infty}^{\infty} dx \int_{-\infty}^x d\tilde{x} \exp\left(-\frac{x^2 + \tilde{x}^2}{2(\sigma^{AB})^2}\right) \exp\left(\frac{x\tilde{x}}{(\sigma^{AB})^2}\right) \exp\left(-\frac{x^2 + \tilde{x}^2}{(\sigma^{BC})^2}\right) \exp\left(-\frac{x^2 - \tilde{x}^2}{2d^{BC}v}\right) \right. \\
&\quad \left. + \int_{-\infty}^{\infty} dx \int_x^{\infty} d\tilde{x} \exp\left(-\frac{x^2 + \tilde{x}^2}{2(\sigma^{AB})^2}\right) \exp\left(\frac{x\tilde{x}}{(\sigma^{AB})^2}\right) \exp\left(-\frac{x^2 + \tilde{x}^2}{(\sigma^{BC})^2}\right) \exp\left(-\frac{\tilde{x}^2 - x^2}{2d^{BC}v}\right) \right)^2 \\
&= \frac{\kappa_{\Delta}^{BC}}{\pi^2(\sigma^{BC})^4} \left(\int_{-\infty}^{\infty} dx \exp\left(-\frac{x^2}{\beta}\right) \int_{-\infty}^x dx \exp\left(-\frac{\tilde{x}^2}{\tilde{\beta}}\right) \exp\left(\frac{x\tilde{x}}{(\sigma^{AB})^2}\right) \right. \\
&\quad \left. + \int_{-\infty}^{\infty} dx \exp\left(-\frac{x^2}{\tilde{\beta}}\right) \int_x^{\infty} dx \exp\left(-\frac{\tilde{x}^2}{\beta}\right) \exp\left(\frac{x\tilde{x}}{(\sigma^{AB})^2}\right) \right)^2
\end{aligned} \tag{100}$$

where $\beta^2 = \frac{2\delta_{\Delta,\varepsilon}^{BC}(\sigma^{AB})^2(\sigma^{BC})^2}{\delta_{\Delta,\varepsilon}^{BC}(\sigma^{BC})^2 + 2\delta_{\Delta,\varepsilon}^{BC}(\sigma^{AB})^2 + (\sigma^{AB})^2(\sigma^{BC})^2}$, and $\tilde{\beta}^2 = \frac{2\delta_{\Delta,\varepsilon}^{BC}(\sigma^{AB})^2(\sigma^{BC})^2}{\delta_{\Delta,\varepsilon}^{BC}(\sigma^{BC})^2 + 2\delta_{\Delta,\varepsilon}^{BC}(\sigma^{AB})^2 - (\sigma^{AB})^2(\sigma^{BC})^2}$, and $\delta_{\Delta,\varepsilon}^{BC} = vd^{BC}\tau_{\varepsilon}$ captures the elements that spread the arrival time of input spikes to the layer C post-synaptic neuron, as well as the spiking time of the post-synaptic neuron. Complete the square in the exponent to obtain

$$\begin{aligned}
\overline{Q_{\Delta,\varepsilon}^{BB}}(x, y) &= \frac{\kappa_{\Delta}^{BC}}{\pi^2(\sigma^{BC})^4} \left(\int_{-\infty}^{\infty} dx \exp\left(-x^2 \left(\frac{1}{\beta^2} - \frac{\tilde{\beta}^2}{4(\sigma^{AB})^2}\right)\right) \int_{-\infty}^x \left(\frac{1}{\tilde{\beta}^2} - \frac{\beta^2}{4(\sigma^{AB})^2}\right) d\chi \beta \exp(-\chi^2) \right. \\
&\quad \left. + \int_{-\infty}^{\infty} dx \exp\left(-x^2 \left(\frac{1}{\tilde{\beta}^2} - \frac{\beta^2}{4(\sigma^{AB})^2}\right)\right) \int_x^{\infty} \left(\frac{1}{\beta^2} - \frac{\tilde{\beta}^2}{4(\sigma^{AB})^2}\right) d\tilde{\chi} \tilde{\beta} \exp(-\tilde{\chi}^2) \right)^2 \\
&= \frac{\kappa_{\Delta}^{BC}}{\pi^2(\sigma^{BC})^4} \left(\int_{-\infty}^{\infty} dx \exp\left(-x^2 \left(\frac{1}{\beta^2} - \frac{\tilde{\beta}^2}{4(\sigma^{AB})^2}\right)\right) \left(1 + \operatorname{erf}\left(x \left(\frac{1}{\beta^2} - \frac{\tilde{\beta}^2}{4(\sigma^{AB})^2}\right)\right)\right) \right. \\
&\quad \left. + \int_{-\infty}^{\infty} dx \exp\left(-x^2 \left(\frac{1}{\tilde{\beta}^2} - \frac{\beta^2}{4(\sigma^{AB})^2}\right)\right) \left(1 - \operatorname{erf}\left(x \left(\frac{1}{\tilde{\beta}^2} - \frac{\beta^2}{4(\sigma^{AB})^2}\right)\right)\right) \right)^2 \\
&= \frac{\kappa_{\Delta}^{BC}}{\pi^2(\sigma^{BC})^4} \left(\int_{-\infty}^{\infty} dx \exp\left(-x^2 \left(\frac{1}{\beta^2} - \frac{\tilde{\beta}^2}{4(\sigma^{AB})^2}\right)\right) \right) + \int_{-\infty}^{\infty} dx \exp\left(-x^2 \left(\frac{1}{\tilde{\beta}^2} - \frac{\beta^2}{4(\sigma^{AB})^2}\right)\right) \\
&= \frac{\kappa_{\Delta}^{BC}}{\pi^2(\sigma^{BC})^4} \tilde{\beta}^2 \left(\frac{1}{\beta^2} - \frac{\tilde{\beta}^2}{4(\sigma^{AB})^2}\right) + \beta^2 \left(\frac{1}{\tilde{\beta}^2} - \frac{\beta^2}{4(\sigma^{AB})^2}\right).
\end{aligned} \tag{101}$$

Substituting in the definitions for β and $\tilde{\beta}$ gives

$$\overline{Q_{\Delta,\varepsilon}^{BB}} = \kappa_{\Delta}^{AB} \frac{4 \left(2 + \frac{(\sigma^{BC})^2}{(\sigma^{AB})^2}\right)}{\left(\frac{(\sigma^{BC})^2}{\delta_{\Delta,\varepsilon}^{BC}} - 2\right) \left(\frac{(\sigma^{BC})^2}{\delta_{\Delta,\varepsilon}^{BC}} - 2 - 2\frac{(\sigma^{BC})^2}{(\sigma^{AB})^2}\right) \left(\frac{(\sigma^{BC})^2}{\delta_{\Delta,\varepsilon}^{BC}} + 2 + \frac{(\sigma^{BC})^2}{(\sigma^{AB})^2}\right)}. \tag{102}$$

The final expression for mean covariance between pre-synaptic inputs on arrival at the post-synaptic neuron is a function of three main components: the ratio of the radial propagation delay to inter-laminar propagation delay between layers A and B , captured in κ_{Δ}^{AB} , the ratio of the connectivity radii between each layer, $\frac{(\sigma^{BC})^2}{(\sigma^{AB})^2}$, and the ratio of the connectivity radius between layers B and C to the inter-laminar propagation constant, $\delta_{\Delta,\varepsilon}^{BC}$, where $\delta_{\Delta,\varepsilon}^{BC} = vd^{BC}\tau_{\varepsilon}$ (see Section 3.4), which captures the impact of propagation delay between layers B and C .

References

M. M. Asl, A. Valizadeh, and P. A. Tass. Dendritic and axonal propagation delays determine emergent structures of neuronal networks with plastic synapses. *Scientific Reports*, 7, 2017.

- A. N. Burkitt, H. Meffin, and D. B. Grayden. Study of neuronal gain in a conductance-based leaky integrate-and-fire neuron model with balanced excitatory and inhibitory synaptic input. *Biological Cybernetics*, 89:119–125, 2003.
- A. N. Burkitt, H. Meffin, and D. B. Grayden. Spike-timing dependent plasticity: the relationship to rate-based learning for models with weight dynamics determined by a stable fixed point. *Neural Computation*, 16:885–940, 2004.
- A. N. Burkitt, M. Gilson, and J. L. van Hemmen. Spike-timing-dependent plasticity for neurons with recurrent connections. *Biological Cybernetics*, 96:533–546, 2007.
- C. E. Carr and M. Konishi. Axonal delay lines for time measurement in the owl’s brainstem. *Proceedings of the National Academy of Sciences, USA*, 85:8311–8315, 1988.
- C. E. Davey, D. B. Grayden, and A. N. Burkitt. General analytical solution to Linsker’s application of Hebbian rules in neural networks. *Arxiv preprint*, pages 1–20, 2018.
- A. Eguchi, S. A. Neymotic, and S. M. Stringer. Color opponent receptive fields setl-organize in a biophysical model of visual cortex via spike-timing dependent plasticity. *Frontiers in Neural Circuits*, 8(16), 2014.
- W Gerstner, R. Kempter, J. L. van Hemmen, and H. Wagner. A neuronal learning rule for sub-millisecond temporal coding. *Nature*, 383:76–78, 1996.
- I. S. Gradshteyn and I. M Ryzhik. *Table of integrals, series and products*, chapter 7, page 810. Elsevier, 7th edition, 2007.
- T. Kato. *Perturbation Theory for Linear Operators*, chapter 6, pages 1–643. Springer, second edition, 1995.
- R. Kempter, W. Gerstner, and J. L. van Hemmen. Hebbian learning and spiking neurons. *Physical Review E*, 59(4):4498–4514, 1999a.
- R. Kempter, W. Gerstner, and J. L. van Hemmen. Spike-based compared to rate-based Hebbian learning. *Advances in Neuron Information Processing Systems*, 11:128–131, 1999b.
- J. Kremkow, L. U Perrinet, C. Monier, JM. Alonso, A. Aertsen, Y. Frégnac, and G. S. Masson. Push-pull receptive field organization and synaptic depression: Mechanisms for reliably encoding naturalistic stimuli in V1. *Frontiers in Neural Circuits*, 11:10–37, 2016.
- R. Kumar. *Signals and systems*. PHI Learning Pvt. Ltd., 2009.
- C. Leibold and C. L. van Hemmen. Temporal receptive fields, spikes, and Hebbian delay selection. *Neural Networks*, 14: 805–813, 2001.
- C. Leibold, R. Kempter, and C. L. van Hemmen. How spiking neurons give rise to a temporal-feature map: From synaptic plasticity to axonal selection. *Physical Review E*, 65:1–20, 2001.
- R. Linsker. From basic network principles to neural architecture: Emergence of spatial-opponent cells. *Proceedings of the National Academy of Sciences, USA*, 83:7508–7512, 1986a.
- R. Linsker. From basic network principles to neural architecture: Emergence of orientation-selective cells. *Proceedings of the National Academy of Sciences, USA*, 83:7508–7512, 1986b.
- R. Linsker. From basic network principles to neural architecture: Emergence of orientation columns. *Proceedings of the National Academy of Sciences, USA*, 83:7508–7512, 1986c.
- D. J. MacKay and K. D. Miller. Analysis of Linsker’s application of Hebbian rules to linear networks. *Network*, 1:257–297, 1990.
- K. D. Miller. *Correlation-based models of neural development*, chapter 7, pages 267–352. Hillsdale, 1990.
- R. J. Pumphrey and J. Z. Young. The rates of conduction of nerve fibres of various diameters in cephalopods. *Journal of Experimental Biology*, 15:453–466, 1938.
- M. Saam and R. Eckhorn. Lateral spike conduction velocity in the visual cortex affects spatial range of synchronisation and receptive field size without visual experience: a learning model with spiking neurons. *Biological Cybernetics*, 83:L1–L9, 2000.

- R. Sinha, M. Hoon, J. Baudin, H. Okawa, R. Wong, and F. Rieke. Cellular and circuit mechanisms shaping the perceptual properties of the primate fovea. *Cell*, 168(3):413–426, 2017.
- L. Thibos, D. Still, and A. Bradley. Characterization of spatial aliasing and contrast sensitivity in peripheral vision. *Vision Research*, 36:249–258, 1996.
- J. L. van Hemmen. *Spike-timing dependent plasticity models*, chapter 1, pages 269–275. Elsevier, 2009.
- A. Venkataraman, P. Lewis, P. Unsbo, and L. Lunstrom. Peripheral resolution and contrast sensitivity: Effects of stimulus drift. *Vision Research*, 133:145–149, 2017.
- V. Virsu, J. Rovamo, P. Laurinen, and R. Nasanen. Temporal contrast sensitivity and cortical magnification. *Vision Research*, 22:1211–1217, 1982.
- S. Wimbauer, O. G. Wensch, K. D. Miller, and J. L. van Hemmen. Development of spatiotemporal receptive fields of simple cells: II. Simulation and analysis. *Biological Cybernetics*, 77:463–477, 1997.
- S. Wimbauer, W. Gerstner, and J. L. van Hemmen. Analysis of a correlation-based model for the development of orientation-selective receptive fields in the visual cortex. *Network: Computation in Neural Systems*, 9:449–466, 1998.
- C. Zhao, R. Hata, J. Okamura, and G. Wang. Differences in spatial and temporal frequency interactions between central and peripheral parts of the feline area 18. *Cognitive Neuroscience*, 44(8):2635–2645, 2016.